HHS Public Access

Author manuscript

Neuron. Author manuscript; available in PMC 2022 July 07.

Published in final edited form as:

Neuron. 2021 July 07; 109(13): 2116–2130.e6. doi:10.1016/j.neuron.2021.05.006.

A locus coeruleus to dentate gyrus noradrenergic circuit modulates aversive contextual processing

Dong-oh Seo[#1], **Eric T. Zhang**[#2,3,4], **Sean C. Piantadosi**[3,4], **David J. Marcus**[3,4], **Laura E. Motard**[1], **Bryce K. Kan**[3,4], **Adrian M. Gomez**[1], **Tammy K. Nguyen**[3,4], **Li Xia**[5], **Michael R. Bruchas**[1,2,3,4,5,6,7,†]

[1]Department of Anesthesiology, Division of Basic Research, Washington University School of Medicine, St. Louis, MO 63110, USA

[2]Department of Bioengineering, University of Washington, Seattle, WA 98105, USA

[3]Department of Anesthesiology and Pain Medicine, University of Washington, Seattle, WA, 98195, USA

[4]Center for the Neurobiology of Addiction, Pain and Emotion, University of Washington, Seattle, WA, 98195, USA

[5]Division of Biology and Biomedical Sciences, Washington University School of Medicine, St. Louis, Missouri 63110, USA

[6]Departments of Anesthesiology and Pharmacology, University of Washington, Seattle, WA, 98195, USA

[7]Lead Contact

[#] These authors contributed equally to this work.

Abstract

Dysregulation in contextual processing is believed to affect several forms of psychopathology, such as post-traumatic stress disorder (PTSD). The dentate gyrus (DG), a subregion of the

[†]Correspondence to: Michael R. Bruchas, Ph.D. (mbruchas@uw.edu).

Current address for D.S.: Department of Neurology, Washington University School of Medicine, St. Louis, MO 63110.

Author contributions: D.S. performed conceptualization, methodology, investigation, formal analysis, writing of the original draft, review. E.T.Z. performed conceptualization, methodology, investigation, formal analysis, imaging data analysis, writing of the original draft, review. S.C.P. performed imaging data analysis, writing of the original draft, review. D.J.M. performed electrophysiological experiments, writing of the original draft. L.E.M. performed behavioral experiments, immunohistochemistry, surgeries. B.K.K. performed immunohistochemistry, behavioral analysis. A.M.G performed in-situ hybridization. L.X. performed imaging data analysis. T.K.N. performed immunohistochemistry. M.R.B. conceptualized, acquired funding for, and supervised the project, as well as assisted in writing the manuscript.

Declaration of interests: The authors declare no competing interests.

Inclusion and Diversity: We worked to ensure sex balance in the selection of non-human subjects. One or more of the authors of this paper self-identifies as an underrepresented ethnic minority in science. One or more of the authors of this paper received support from a program designed to increase minority representation in science. The author list of this paper includes contributors from the location where the research was conducted who participated in the data collection, design, analysis, and/or interpretation of the work.

Data and materials availability: All data is available in the manuscript or the supplementary materials.

hippocampus, is thought to be an important brain region for disambiguating new experiences from prior experiences. Noradrenergic (NE) neurons in the locus coeruleus (LC) are more tonically active during stressful events and send dense projections to the DG, yet an understanding of their function in DG-dependent contextual discrimination has not been established. Here, we isolate a key function of the LC-NE-DG circuit in contextual aversive generalization using selective manipulations and in vivo single cell calcium imaging. We report that activation of LC-NE neurons and terminal activity results in contextual generalization. We found these effects required β-adrenergic-mediated modulation of hilar interneurons to ultimately promote aversive generalization, suggesting that disruption of noradrenergic tone may serve as an important avenue for treating stress-induced disorders.

Graphical Abstract

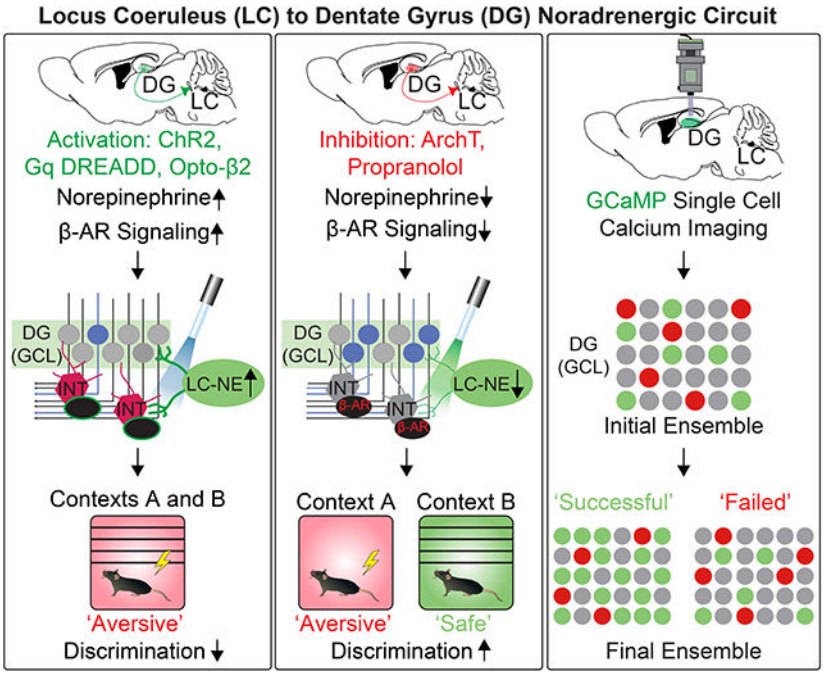

eTOC

Seo and Zhang et al. implicate a locus coeruleus to dentate gyrus noradrenergic circuit in modulation of aversive contextual processing. Disrupted contextual processing occurs in several psychopathologies, including post-traumatic stress disorder (PTSD). Elucidating the role of noradrenergic modulation of behavior can yield more effective treatments for stress disorders.

Keywords

hippocampus; dentate gyrus; locus coeruleus; norepinephrine; fear conditioning; learning and memory; optogenetics; calcium imaging; neuromodulation; beta-adrenergic

Introduction

Post-traumatic stress disorder (PTSD) and other anxiety disorders are commonly characterized by the dysregulation of fear responses due to abnormal information processing, such as fear overgeneralization (Liberzon and Abelson, 2016). Individuals with anxiety disorders experience heightened levels of fear in response to cues that remind them of the initial threat. This fear generalization is a critical adaptive behavior to avoid danger in a constantly changing environment. However, excessive fear generalization can cause maladaptive fear responses to innocuous cues and can severely impact daily functioning (Siegmund and Wotjak, 2006; Hennings et al. 2020). In fact, recent studies have shown that generalization in learned contextual fear has greater implications in the etiology of a wide range of PTSD symptoms, such that a safe environmental context may be perceived as a dangerous or threatening context, leading to hypervigilance and exaggerated threat detection (Kheirbek et al., 2012; Besnard and Sahay, 2016).

Many studies have shown that the hippocampus is a critical neural structure for processing environmental information during a new episodic event (Morris, 2006; Lisman et al., 2017; O'Reilly and McClelland, 1994). Computational and behavioral studies have suggested that the dentate gyrus (DG), a subregion of the hippocampus, has an essential role in this process. This is particularly true when new information is similar to existing knowledge, because the DG engages in sparse coding of incoming information from the entorhinal cortex (EC) (O'Reilly and McClelland, 1994; Treves et al., 2008; McHugh et al., 2007; Deng et al., 2013). During this process, granule cells in the DG send signals to the CA3 region of the hippocampus, where pattern completion, a process that recalls memory through partial cues, occurs (Nakazawa et al., 2002). The unique anatomical characteristics of the DG have led to the idea that it is a neural structure essential for pattern separation, which is a process that discriminates amongst similar stimuli (O'Reilly and McClelland, 1994; Marr, 1971). However, it is currently unknown how specific neuromodulators alter DG activity during aversive experiences and contribute to overgeneralization of fear.

The DG receives dense neuromodulatory input from norepinephrine (NE) cell projections in the locus coeruleus (LC) (Blackstad et al., 1967). The LC is highly active during stressful events in rodents and primates and promotes behavioral responding under a gradient of arousal states (McCall et al., 2015; Valentino and Van Bockstaele, 2008). Physiological studies suggest that NE is involved in perforant path synaptic plasticity via modulating neuronal activities of dentate granule cells and/or local interneurons. This supports the hypothesis that the LC-NE system plays a role in DG-dependent learning and memory (Harley, 2007; Walling and Harley, 2004; Seidenbecher et al., 1997; Rose and Pang, 1989).

Despite these converging lines of molecular and physiological data, the precise relationship between the function of the DG, and neuromodulation by the LC-NE system in processing fear-related information remains unclear. Here we conducted an integrated neuromodulatory circuit analysis approach, combining viral tracing, opto- and chemo-genetic tools, and *in vivo* Ca^{2+} imaging with a well-established Pavlovian contextual fear discrimination (CFD) paradigm in which animals were placed in two similar, but different, contexts daily (McHugh et al., 2007; Lovett-Barron et al., 2014; Danielson et al. 2016). Elucidating

the relationship between the LC-NE system and DG-dependent contextual processing is relevant to efforts to prevent dysregulation of contextual processing in anxiety and other stress-related disorders, such as PTSD.

Results

LC-DG Circuit Excitation and Inhibition Drive Opposing Learning States

The LC is highly active during stressful events, so we first photo-activated LC-DG projections during CFD training. Cre-recombinase dependent viral vectors containing the light-sensitive cation channel channelrhodopsin-2 (ChR2) were injected unilaterally into the LC of Th-cre mice (Fig. 1A). We have previously reported that >98% of ChR2-eYFP cells in the LC of Th-cre mice co-express dopamine-beta-hydroxylase, the precursor for NE synthesis (McCall et al., 2015). To examine the axonal projection of the $ChR2^+$ LC cells into the hippocampus, we imaged ChR2-eYFP-expressing fibers and quantified the density of the $ChR2^+$ axons in the sub-regions of the hippocampus. $ChR2^+$ LC fibers were observed throughout dorsal hippocampus (Fig. 1A-B). The major sub-regions of the hippocampus (DG, CA1, and CA3) showed similar density of $ChR2^+$ fibers (Fig 1C). To anatomically confirm the LC to DG projection circuit and potential tropism issues, we conducted a series of complimentary retro-viral tracing techniques, injecting either Cholera Toxin B subunit (CTB) or a retrogradely trafficked adeno associated virus (AAV) into the DG (Tervo et al., 2016). This DG-specific retrotracing revealed that Th^+ LC neurons are indeed a pre-synaptic input (Fig. 1B).

To mimic the ‘high-tonic’ LC cell firing that occurs in stressful events (McCall et al., 2015; Valentino and Van Bockstaele, 2008), 8 Hz-pulsed photostimulation was delivered bilaterally above the DG during contextual fear conditioning (Fig. 1D). A control group of mice (ChR2(−)) lacking Cre-recombinase and mice with acute activation of the LC-DG projection (Th-$Cre^{LC\text{-}DG}$::ChR2) were tested in this paradigm. Freezing levels between context A (unsafe) and context B (safe) were compared for both groups of mice across training days 1, 5, and 9 to reveal interactions between optogenetic treatment and contexts across CFD training. While no differences between Th-$Cre^{LC\text{-}DG}$::ChR2 and ChR2(−) mice were present in the beginning of training paradigm, there were significant and robust differences in freezing behavior at the end of training (Fig. 1E). Only the control group of animals successfully discriminated between the two similar contexts, while Th-$Cre^{LC\text{-}DG}$::ChR2 animals demonstrated impaired performance in discrimination on days 5 and 9 of training. Comparison of freezing levels for all training days showed a similar trend of improvement during the middle and late stages of training (Fig. S1A-B). Additionally, there were no significant differences in freezing in context A when comparing wild-type controls to Th-$Cre^{LC\text{-}DG}$::ChR2 mice. These results suggest that activation of LC-DG projections facilitates contextual fear generalization without affecting the ability to learn the aversive association. This fear generalization persisted even when animals were subjected to CFD training using two very different contexts (Fig. S1M-Q) and was likely not due to differences in basal anxiety level of the transgenic background (Fig. S2B-E). By comparison, mice injected with a control fluorophore showed freezing levels similar to ChR2(−), indicating that differences in freezing levels were not due to the viral

injection procedure (Fig. S1E-G). Further, when contexts were presented in a randomized order, animals again showed an impairment of CFD throughout training with the LC activation (Fig. S1P-Q). These results indicate that the LC-DG circuit is associated with disambiguating similar contexts (Fig. S1M-O).

Next, to test whether the LC-NE system is necessary for modulating DG function in contextual fear discrimination, we optogenetically inhibited LC-DG projections using archaerhodopsin (ArchT), a light-sensitive proton pump (Fig. 1F) (Han et al., 2011). To engage the facilitation effect of discrimination, the contextual fear conditioning paradigm was made more difficult by randomizing the order of the two similar contexts (Fig. 1G). With this randomly ordered CFD task, there were no significant differences through the middle phase of training, likely due to the removal of the predictive cue of daily context order. However, by the end of training, there was a significant difference in behavior between wild-type controls (ArchT(−)) and mice with acute inhibition of the LC-DG projection (Th-Cre$^{LC\text{-}DG}$::ArchT) (Fig. 1H). In this CFD paradigm, control groups of mice struggled to discriminate between the two similar contexts, while Th-Cre$^{LC\text{-}DG}$::ArchT mice froze significantly more in context A (unsafe) than in context B (safe). Freezing levels between context A and B were compared across all training days, again showing a difference in freezing between Th-Cre$^{LC\text{-}DG}$::ArchT mice and wild-type controls (Fig. S1C-D). On the other hand, in the one-trial contextual fear conditioning paradigm, the LC-DG inhibition affected neither acquisition nor retrieval of the contextual information itself (Fig. S1H-I). These results indicate that inhibition of the LC-DG projections reduces contextual fear generalization and facilitates disambiguation.

In Vivo Calcium Imaging During Contextual Fear Discrimination Reveals Changes in DG Ensemble Dynamics

We next examined whether a DG neuronal ensemble encodes the dynamic behavioral states during CFD training, utilizing in vivo calcium imaging by injecting an AAV expressing the genetically encoded calcium indicator, GCaMP6f, driven by CamKII promoter, into the DG, followed by the implantation of a micro-endoscopic GRIN lens to monitor neuronal ensemble changes (Fig. 2A-B, Fig. S3A-B). In addition, while neuronal activity of GCs in the DG was monitored, LC-NE activity was increased by the expression of Cre-dependent excitatory designer receptor exclusively activated by designer drugs (DREADD) infection in LC-NE (Th^{+}) neurons. The DREADD agonist clozapine-N-oxide (CNO) was then injected prior to imaging (Fig. 3A-C). Control, wild-type mice were treated in the same way with DREADD and CNO during the CFD paradigm (Fig. 2A-C).

When wild-type controls (HM3Dq(−); Fig. 2) underwent contextual fear conditioning, we successfully recorded and segmented responses of individual neurons in the GCL (Fig. 2D-F). For each day of training, individual neurons were classified as preferentially active in context A, context B, or not selective for context (Fig. 2H). This was achieved by conducting a two-sample *t*-test of Z-scored fluorescence traces from context A and context B with an alpha level of $p < 0.05$. To validate this methodology, we compared average activity while in both contexts and response amplitude in both contexts of cells that were classified as either selective to context A or context B. In both cases, neurons showed significant

differences in activity preferential towards the context they were classified in (Fig. 2I, Fig. S3F-H). Cells selective to context A (unsafe) demonstrated markedly higher activity and response amplitude in context A compared to context B (safe), and cells selective to context B displayed the opposite trend in activity, further substantiating this classification approach. There were no significant context specific shifts in response amplitude among classified cells during the training.

In wild-type controls, we observed an increase in cells selectively responding to context B (safe) over the course of CFD training (Fig. 2K). This suggests that as mice learn to distinguish between context A (unsafe) and context B (safe), their behavioral output is matched by a subsequent shift in DG-GC ensemble dynamics towards context B (Fig. 2G). Mice that were able to avoid generalization and encode ambiguous cues separately from threatening cues experience an increased recruitment in cells responding to context B (safe) (Fig. 2J). On the first day of training, wild-type controls at first generalized between context A (unsafe) and context B (safe) together. However, as they learned to disambiguate cues related to context B (safe) and had a similar proportion of neurons responding in each context. However, as they learned to disambiguate cues relating to context B (safe) from threatening cues related to context A (unsafe), a significantly increased population of neurons was recruited to respond in that context (Fig. 2L). These results suggest that as wild-type mice successfully improve their performance in the CFD task, GC ensemble dynamics in the DG shift to reflect this change in behavior, with an increased recruitment of neurons responding to context B (safe) as the recognition of that context increases.

To quantify this potential correlation, we calculated a ratio between the proportion of cells responding selectively to either context A (unsafe) or B (safe) for each mouse at both the beginning and end of training, as well as the proportion of freezing behavior in context B (safe) compared to context A (unsafe). We used linear regression and Pearson correlation to assess the link between these ratios for both the beginning and end of training (Fig. 2M). While there is little to no relationship between the two variables at the beginning of training, by the end of the task this shifts to a significant fit between cell selectivity ratio and freezing ratio in the two contexts. These data further indicate that as mice are better able to disambiguate the two distinct contexts, a corresponding shift in DG-GC ensemble activity occurs proportional in strength to their discrimination ability in the task. It also indicates that the effect seen in the DG ensemble is not driven by a single mouse, but rather that the cohort as a whole show consistent increases in context B cells across training.

We also determined whether the DG ensemble shifted when looking only at cells that were identified both at the beginning and the end of training (Fig. 2N). Here we report a nearly identical effect occurs compared to the general population of imaged cells, whereby there is an increased population of neurons responding in context B (safe) over the course of the training (Fig. 2O). In addition, we also examined shifts in individual cell selectivity over the course of the training, to determine whether high percentages of neurons tended to shift from a particular selectivity at the beginning of training to a different selectivity at the end of training (Fig. 2P). This was done by dividing neurons into nine different categories based on their selectivity on day 1 and day 9 of training. A high percentage (~42%) of neurons responding selectively to context B (safe) at the beginning of training remained selective

to that context at the end of training, and a high percentage (~49%) of neurons responded selectively to context A (safe) at the beginning of training and then selectively to context B (safe) by the end of training. These data further corroborate our findings of a shift in DG GC ensemble in wild-type mice during the course of the training.

These results suggest that neurons that responded selectively to context B (safe) at the beginning of training tended to remain selective to that context. However, neurons that responded selectively to context A (unsafe), and neurons that responded nonselectively, at the beginning of training were recruited to respond in context B (safe) as mice disambiguate the cues related to that context.

Activation of LC-DG Circuit During *In Vivo* Calcium Imaging Impairs DG Ensemble Dynamics

Use of calcium imaging techniques allowed us to determine that wild-type mice that were able to successfully discriminate between the two similar contexts experience a specific pattern shift of GC ensemble dynamics in the DG. We next sought to understand how increased LC-NE activity, which is sufficient to produce fear generalization (Fig. 1E), impacts the context specific changes in GC ensemble activity. We utilized *in vivo* calcium imaging in the DG while controlling activity from the LC chemogenetically in Th-Cre mice (Fig. 3A-B, Fig. S3A-B). These mice then underwent the CFD task following intraperitoneal injections of the DREADD agonist CNO (Fig. 3C) which allowed us to capture precise neural ensemble dynamics in Th-Cre$^{LC\text{-}DG}$::HM3Dq mice while eliciting increased tonic LC activity Similar to what we observed with optogenetic activation of the LC-DG projection (Fig. S1A), we observed that wild-type controls were able to successfully disambiguate the two similar contexts, while Th-Cre$^{LC\text{-}DG}$::HM3Dq mice were unable to do so effectively (Fig. 3D). These data indicate that the microendoscope implantation and miniature microscope weight did not interfere with the expression of behavior in the CFD task and that tonic LC activation via DREADDs produces context generalization. Additionally, Th-Cre$^{LC\text{-}DG}$::HM3Dq mice treated with saline had lower freezing in context B (safe) compared to context A (unsafe) than Th-Cre$^{LC\text{-}DG}$::HM3Dq mice treated with CNO by the end of training. These results establish that differences in freezing levels between the two groups were not due to the transgenic background of the mice (Fig. S3C-E).

Since Th-Cre$^{LC\text{-}DG}$::HM3Dq mice were not able to differentiate between the two different contexts, we hypothesized that DG-GC ensemble dynamics would not shift during chemogenetic LC activation towards context B (safe), as they did in wild-type controls (Fig. 3E). Again, we classified cells imaged during a CFD study as selective to context A, selective to context B, or not selective to either context at the beginning and end of training, based on their relative activity levels in each context (Fig. S3F-H). In this experimental paradigm, we found that wild-type, CNO-injected controls showed increased recruitment of cells responding in context B (safe), however Th-Cre$^{LC\text{-}DG}$::HM3Dq, CNO-injected mice did not display a similar level of elevated neuronal recruitment in the GCL. Th-Cre$^{LC\text{-}DG}$::HM3Dq mice had equal amounts of neuronal activity in context A and context B on both the first and last days of training (Fig. 3F). Th-Cre$^{LC\text{-}DG}$::HM3Dq mice were not able differentiate between the two contexts, while the neuronal ensemble activity

underwent no significant changes in recruitment for either context (Fig. 3G-H). These results indicate that unlike wild-type controls, elevated tonic LC activity in Th-Cre$^{LC\text{-}DG}$::HM3Dq mice produces more homogenous DG ensemble activity, and while cell selectivity was maintained on an individual neuron basis, the ensemble as a whole was not able to clearly disambiguate contextual cues, preventing recruitment of new granule cells in the DG.
We next examined the relationship between the behavioral and neural ensemble changes occurring in Th-Cre$^{LC\text{-}DG}$::HM3Dq mice. There was no correlation between A:B cell selectivity ratio and B:A behavioral response ratio in Th-Cre$^{LC\text{-}DG}$::HM3Dq mice on both days 1 and 9, suggesting that poor context discrimination caused by elevated LC activity is associated with a lack of a shift in DG-GC neuron activity towards context B (safe; Fig. 2M).

We next investigated the DG-GC ensemble shifts in Th-Cre$^{LC\text{-}DG}$::HM3Dq mice when looking only at cells that were identified both at the beginning and the end of training (Fig. 3J). Within this stably tracked population of neurons, we observed that over the course of training there is a significant decrease in neurons responding to context A (unsafe), and an increase in neurons responding to context B (safe) (Fig. 3L). We also examined shifts in individual cell selectivity over the course of the training, to determine whether neurons tended to shift from a particular selectivity at the beginning of training to a different selectivity at the end of training (Fig. 3K). This was done by dividing neurons into nine different categories based on their selectivity on day 1 and day 9 of training. A moderate percentage (~31%) of neurons responding selectively to context A (unsafe) at the beginning of training remained selective to context A at the end of training, while a high percentage (~39%) of neurons responding selectively towards context B remained selective to context B at the end of training. These results corroborate our other findings regarding the failure of the DG GC ensemble to shift towards the safe context over the course of training.

Comparing normalized cumulative distributions of cell selectivity, we found a significant shift in responsiveness towards context B over the course of the CFD task in wild-type controls, but not in Th-Cre$^{LC\text{-}DG}$::HM3Dq mice, whose responsiveness remains stable throughout training. (Fig. 3M). This further supports the conclusion that elevated LC activity during CFD training prevents recruitment of new DG GCs in context B (safe).

Optical Stimulation of a Chimeric Opsin/β-adrenergic Receptor Expressed by Inhibitory Interneurons Impairs Contextual Fear Discrimination

The impairment of contextual discrimination learning with the activation of the LC-NE system was somewhat unexpected, because it contradicts the view that the LC circuit network facilitates cognitive function and hippocampus dependent memory in general (Sara, 2009; Mair et al., 2005; Kempadoo et al., 2016; Takeuchi et al., 2016; Wagatsuma et al., 2018). To that end, we then attempted to understand the specific mechanisms by which the LC-NE system modulates CFD and hippocampal function. To drive chemogenetic activation of the LC-DG circuit, we used transgenic mice expressing Cre-recombinase driven by dopamine beta-hydroxylase (Dbh-Cre), injected with a Cre-dependent excitatory DREADD (Fig. 4A-B). In this CFD task, animals were injected with CNO intraperitoneally 30 minutes prior to the task each day and starting on the fifth day animals received intraperitoneal

injections of either saline or β-selective antagonist propranolol prior to CNO (Fig. 4C) (Stadel and Lefkowitz, 1991).

In this CFD task, animals with chemogenetic activation of the LC-DG circuit receiving saline injections were unable to discriminate between context A (unsafe) and context B (safe) across all phases of training (Fig. 4D). Meanwhile, animals with chemogenetic activation of the LC-DG circuit receiving β-selective antagonist propranolol injections successfully discriminated between the two contexts on day 9 of training. This result suggests that modulation of aversive contextual memory occurs via norepinephrine engagement of β-signaling in the DG, while blocking these receptors leads to recovery of discrimination ability even with activation of the LC-NE system.

Based on the results above, we considered several possible explanations for how the LC-NE system may be influencing the DG neural ensemble during CFD (Fig. 4E). Evidence exists that β-adrenergic receptors are critical for establishing LC-NE synaptic plasticity in the DG (Walling and Harley, 2004; Lethbridge et al., 2014; Hagena et al., 2016), and thus represent a likely candidate for the altered recruitment of DG ensembles by LC-NE input.

We therefore examined the expression of Adrb2 on different cell types in the DG. *In-situ* hybridization revealed that most vGAT^{+} interneurons in the DG (~85%) express β_2-AR mRNA, as do most vGlut1^{+} neurons in the DG-GCL (~85%) (Fig. 4F-G). Because Adrb2 is heavily co-expressed with both vGat and vGlut1 in the DG, we posited that LC-NE projections synapsing onto one or both cell types could be modulating contextual generalization in response to LC-NE release into the DG. To evaluate the role of selective engagement of β_2-AR signaling on excitatory neurons in the GCL in modulating performance in the CFD task, we used an AAV virus we previously developed with a DIO construct containing the photo-sensitive β_2-AR-YFP (Fig. 4H). Due to the complexity of expression and temporal limitations of pharmacological approaches in this CFD task to isolate specific receptors in the region, this tool afforded us localized control of signaling, and we have previously demonstrated that it mimics β-AR signaling in vitro and in vivo (Siuda et al., 2015). To selectively target vGlut1^{+} neurons in the GCL, we used transgenic mice expressing Cre-recombinase driven by vesicular glutamate transporter 1 (vGlut1-Cre) (Fig. 4I-K). With this neuromodulatory optogenetic approach, photostimulation of Opto-β_2 acts to mimic β_2-AR signaling in granule cells during the CFD task.

In the CFD task, both the control group (Opto-β_2(−)) and mice with acute activation of the Opto-β_2-AR (vGlut1-Cre^{DG}::Opto-β_2) in GC showed similar levels of freezing in context B (safe) and context A (unsafe) at the beginning of training (Fig. 4L). However, by the end of training, both groups of mice were able to successfully discriminate between the two separate contexts, with both groups of mice displaying lower levels of freezing behavior in context B (safe) compared to context A (unsafe). Additionally, there were no significant differences in freezing in context A when comparing wild-type controls to vGlut1-Cre^{DG}::Opto-β_2 mice. These results indicate that activation of β_2-signaling in excitatory neurons in the DG GCL is likely not the mechanism by which the LC-NE system alters this behavior.

Considering that GCs in the DG receive strong tonic inhibition from local interneurons, one possible interpretation of the results showing enhanced discrimination is that local interneurons that tonically inhibit GCs are inhibited after suppressing NE release in the LC (Fig. 4E) (Houser, 2007). This led to the hypothesis that activation of β-adrenergic signaling within interneurons of the DG may act to impair performance in the CFD task. To assess the ability of β-signaling to alter influence the excitability of DG vGAT^{+} neurons, we first performed a series of electrophysiological experiments. Transgenic mice expressing Cre-recombinase driven by vesicular GABA transporter (vGAT-Cre) and injected with a Cre-recombinase dependent viral vector containing YFP were used to selectively target interneurons in the DG. Using whole-cell patch clamp, we monitored evoked action potential firing in vGAT^{+} neurons (YFP labeled) in the presence of the β-selective agonist isoproterenol, or the β-selective antagonist propranolol (Stadel and Lefkowitz, 1991). We found that isoproterenol significantly increased the excitability of vGAT^{+} neurons at low threshold depolarizations while propranolol diminished the excitability of these neurons (Fig. 4M-O).

With these findings in mind, we targeted DG interneurons using vGAT-Cre mice in the hilus with Cre-dependent Opto-β_2-YFP (Fig. 4P-Q). The control group (Opto-β_2(−)) showed significantly higher freezing in context A (unsafe) compared to context B (safe) during contextual fear discrimination. However, as training progressed, mice with acute activation of the opto-β_2-AR (vGAT-Cre^{DG}::Opto-β_2) in hilus vGAT interneurons displayed no significant differences in freezing between the two contexts (Fig. 4R). Further analysis found that, halfway through training, both groups failed to discriminate between the contexts. However, by the end of training, Opto-β_2(−) mice froze more in context A than B, in contrast to vGAT-Cre^{DG}::Opto-β_2 mice (Fig. 4R). However, vGAT-Cre mice injected with ChR2 instead of Opto-β_2 in the DG displayed a significant different in freezing between context A and context B over the course of training, as did the corresponding wild-type controls (Fig. S4C-E). This indicates that inhibition of freezing in the CFD was not due solely to the presence of optogenetic stimulation, but rather the specific beta-signaling driven by Opto-β_2. Additionally, quantification of Opto-β_2 infection in the GCL and hilus of vGlut1-Cre mice and vGAT-Cre mice showed sufficient infection of the GCL and low infection of the hilus in vGlut1-Cre mice, and sufficient infection of the hilus and low infection of the GCL in vGAT-Cre mice (Fig. S4F-G). Lastly, we found no significant differences in freezing in context A when comparing wild-type controls to vGAT-Cre^{DG}::Opto-β_2 mice. These results indicate that activation of β-AR signaling on vGAT neurons results in impaired CFD, consistent with the hypothesis that local interneurons in the DG are regulated by noradrenergic signaling, to regulate distinguishing of similar information from prior stressful experiences.

Restraint Stress Contributes To The Impairment of Contextual Fear Discrimination

The LC-NE system is highly responsive to stress (McCall et al., 2015; Valentino and Van Bockstaele, 2008). The facilitation effect of contextual fear generalization modulated by the LC-DG circuit is evolutionarily beneficial to survival in stressful contexts. For example, it would be more advantageous to generalize a potentially dangerous context or cue to increase one's chance of survival (Kaouane et al., 2012). We tested if stress exposure mimics the

impairment of CFD as we have seen in the manipulation of the LC-DG system (Fig. 4S-T). Indeed, when animals were treated with restraint stress before the CFD task, they showed impairment in the CFD task consistent with our LC-DG activation experiment, indicated by results that the naïve group of animals showed the significant interaction of Training x Context in freezing, but not Stressed group (Fig. S1J-L). It is important to indicate that there were overall reduction of freezing level in the stressed group, which was not observed in the LC-DG specific manipulation (Fig. 4U). The freezing reduction in the stressed group indicates that the stress manipulation may also recruit other modulators that influence in the performance of fear processing (e.g. glucocorticoid, which impair fear memory processing). These results are consistent with our overarching hypothesis that stressful events activate the LC-NE system, and that stress facilitates contextual fear generalization. In addition, these results further support the more recently proposed functional heterogeneity hypothesis of LC function, and that specific projections to the DG facilitate contextual fear generalization. These results also further support the more recently proposed functional heterogeneity hypotheses of the LC circuit network (Seo and Bruchas, 2017; Uematsu et al., 2017).

Discussion

Here, we report that LC-DG circuit modulates CFD, preventing shifts in new GC recruitments, which is correlated with successful pattern separation, eventually resulting in impairment of CFD. We found that photo-activation of the LC-DG projection in Th-Cre$^{LC\text{-}DG}$::ChR2 mice led to an impairment in performance as CFD training progressed with similar contexts, but not with more pronounced differences between two contexts. Although this remains consistent with the notion that the DG is involved in distinguishing new information that is similar to existing information, our results are somewhat contradictory to the general role of the LC-NE system enhancing memory formation as shown in recent studies demonstrated that optogenetic activation of LC-CA1 and CA3 circuits enhances memory formation (Wagatsuma et al., 2018; Kempadoo et al., 2016; Takeuchi et al., 2016).

Reports examining catecholamine modulation of prefrontal cortical (PFC) cognitive function have suggested that there is an optimal level of catecholamine to achieve the best cognitive performance. Under stress-free conditions, animals with a pharmacological blockade of α_2-adrenergic receptors (e.g., yohimbine), which have high affinity to the NE in the dorsolateral prefrontal cortex, experienced impaired working memory performance (Arnsten 2011). Conversely, pharmacological activation of postsynaptic α_2-adrenergic receptors (e.g., guanfacine) in that region improved working memory performance (Franowicz et al. 2002). Meanwhile, the high levels of NE release induced by stressors suppressed neuronal firing in the PFC via α-1 and β-1 adrenergic receptors, which have low affinity for NE and are thus less likely to get activated in an unstressed condition (Arnsten, 2009; Berridge and Spencer, 2016). While extensive studies have supported this inverted U-shaped relationship between the LC-NE system and PFC dependent working memory performance using operant conditioning paradigms, here we provide evidence that the facilitation of LC-NE cells projecting to the DG impairs contextual fear discrimination and facilitates contextual fear generalization. The fundamental microcircuit structure in the DG involved in pattern separation is likely quite different from recurrent circuits (pyramidal cell to pyramidal cell) in the PFC involved in working memory (Fig. 4E) (Treves et al. 2008). Therefore, the acting

mechanism of the LC-NE system on the DG may be different at the synaptic, cellular, or microcircuit level from the LC-PFC system, and we propose a new mechanism here whereby LC-NE driven inhibitory tone on the GCs prevents pattern separation.

Indeed, this prevention of pattern separation is evident from differences at the ensemble level in the DG in the reliably tracked and the general population of identified cells (Fig. 2K-P, Fig. 3F-M). These results may suggest that as these mice struggle to disambiguate the cues distinguishing the two separate contexts, the DG ensemble similarly struggles and reacts unpredictably, with many cells switching selectivity in a disorganized fashion. While mice with poor discrimination of the contexts due to chemogenetic excitation did have an overall greater proportion of cells with context selectivity than wild-type animals, this may be due to a general increase in activation of DG granule cells produced by pretreatment with CNO prior to training. Additionally, when considering the tracked cell population, it is important to note that this likely does not fully capture DG ensemble shifts, as new cells may be recruited over the course of training to recognize distinct contextual cues. Finally, because of imaging variability of different animals with respect to GCaMP viral expression and the high variability of neurons imaged from each mouse, it is difficult to compare across groups to power a statistical analysis of proportions.

Although the current study suggests that β-adrenergic signaling on inhibitory interneurons plays a major role in the exaggerated fear generalization, the question remains whether β-adrenergic signaling on the interneurons is the exclusive neuromodulatory actor causing fear generalization. Previous studies demonstrated that the primary effect of NE on the GCs in the DG and pyramidal cells in the CA1 is inhibitory and mediated by α_1-adrenergic receptors (Pang and Rose, 1987; Rose and Pang, 1989). It is possible that the failure in discrimination with excessive NE release is due to a synergistic effect of the activation of both α_1- and β_2-adrenergic pathways resulting in suppression of the GCs overall. These possibilities will need to be tested in future studies at the synaptic, cell, and microcircuit levels using high-resolution conditional knockdown approaches.

Additionally, there are many studies that implicate beta-adrenergic receptors on shaping both LTP and LTD in the DG (Milner et al., 2000; Cox et al., 2008; Lethbridge et al. 2014). Evidence suggests that beta-adrenergic activation in the hippocampus induces LTP of perforant path input to the DG (Lethbridge et al., 2014). Few studies have implicated behavioral changes in selected cell types to beta-adrenergic signaling in the manner that we have done here. However, it remains unclear the mechanisms by which beta-adrenergic signaling modulates hippocampal activity during learning and memory. Recent studies have shown enhanced cognitive performance with LC activation of different regions of the hippocampus, but these studies have not demonstrated the U-shaped curve relationship (Wagatsuma et al., 2018; Kaufman et al., 2020). Therefore, future efforts to understand the relationship that LC-NE release concentration and kinetics have on beta-adrenergic signaling onto inhibitory interneurons in the DG. New biosensor tools may help to resolve these issues more definitively (Feng et al., 2019).

Classically, the DG-GC is thought to assist hippocampal processing of a new experience, rather than retrieval, recruiting different subgroups of GCs when the new experience is

similar to a past experience. In a one-trial contextual fear conditioning task we performed, LC-DG manipulation affected neither acquisition nor retrieval of the contextual information itself (Fig. S1H-I). The results we present here indicate that rather than being associated with rapid processing of new episodic memories, the LC-DG circuit is likely to be more involved in differentiating between a prior and new event as they are repeatedly presented. On the other hand, other studies have supported the notion that the adrenergic nervous system mediates emotion-related memory consolidation and reconsolidation (Gazarini et al., 2013; Otis et al., 2015). Recent studies have also reported that LC-NE axons projecting to the hippocampus release dopamine, resulting in enhanced memory consolidation (Wagatsuma et al., 2018; Kempadoo et al., 2016; Takeuchi et al., 2016). In our current study, we sought to control the LC-DG circuits only during the training period, when the contexts were posed to animals. Therefore, it is not clear if the LC-DG system also contributes to the consolidation phase of the learning process, and future studies focused on different phases in memory dynamics (e.g., consolidation, reconsolidation, or after completing long-term CFD) will help to clarify the LC-DG circuit mechanism on the memory process.

With regards to LC-NE inhibition, developing an ideal inhibitory optogenetic tool has been challenging. The light sensitive chloride pump Halorhodopsin (NpHR) was one of the popular tools used in rapidly silencing the activity of neurons. However, it has been reported that NpHR can cause problematic changes in synaptically evoked spiking activity in the period following light activation (Raimondo et al. 2012). Another popular optogenetic silencing tool is archaerhodopsin-3 (Arch), a light-driven outward proton pump, which we chose to use to inhibit the LC-DG circuit in the current study. A recent study reported that sustained Arch photo-activation gradually increased spontaneous neurotransmitter release in the neuronal terminals (Mahn et al., 2016). However, LC-DG terminal inhibition in this report had opposing effects to the activation experiment using ChR2, likely because the rebound effect is low for stimulus durations under a few minutes in length, or differently affected by experimental settings such as light intensity. We also utilized the optogenetic tool Opto-β_2 to mimic wild-type β-adrenergic canonical signaling, as this opto-tool has been characterized in nearly every major known Gs-signaling pathway (Siuda et al., 2015). Indeed, when we injected ChR2 instead of Opto-β_2 in the DG of vGAT-Cre mice, the modulation effect in CFD was not detected (Fig. S4C-E). However, an interesting question remains regarding how this distinct outcome relates to differences in local signaling and resulting physiological changes between the two photo-induced receptors (Opto-β_2 vs. ChR2) in different cell types.

Recent discoveries indicate that neuromodulatory input from LC to hippocampus contributes to processing information pertaining to environmental novelty and spatial tuning (Kempadoo et al., 2016; Takeuchi et al., 2016; Wagatsuma et al., 2018). With the more recent discovery of functional heterogeneity in LC neural circuits, we speculate that LC cells projecting to the DG modulate the DG-dependent pattern separation process, contributing to contextual fear generalization, while LC input to the CA3/CA1 may be involved in the rapid processing of novel contextual information (Wagatsuma et al., 2018). Functional heterogeneity along the septotemporal axis in the hippocampus has also been proposed, and although the basic micro circuitry within the hippocampus is remarkably similar between dorsal and ventral regions, their intersectional connection to the extra-hippocampal structures and their

implicated functions on behavior are known to be quite different along the dorso-ventral axis (i.e. spatial Vs. emotional information). Furthermore, the functional heterogeneity in the DG is also associated with adult hippocampal neurogenesis, a process by which new GCs in the DG are generated and integrated into hippocampal circuitry. An important aspect of hippocampal adult neurogenesis is the distinct physiological characteristics of newborn neurons depending on their ages. A recent study monitoring adult newborn neuron using *in vivo* two-photon calcium imaging within a contextual discrimination task found that young adult born neurons (<6 weeks) display higher rates of neuronal firing than matured neuron, and lower tuning specificity with contextual changes, while mature neurons show more spatial tuning characteristics than young neurons, suggesting that young neurons are more involved in novelty detection rather than spatial tuning (Danielson et al., 2016). They also demonstrated that optogenetic inhibition of the young neurons during exposure to the safe context but not the unsafe context resulted in impairment of contextual fear discrimination, suggesting that young neurons in the dorsal DG are involved in processing the novel safe context. Taken together, it will be important to investigate how LC-NE system functionally modulates the different developmental stages of adult born neurons along dorso-ventral axis.

In clinical studies, it has been reported that PTSD patients fail to perceive both new threats and safe cues accurately, resulting in an impairment in shaping flexible behavioral choices (Liberzon and Abelson, 2016; Lissek et al., 2010). Hypersensitive and inaccurate fear responses may lead to hypervigilance, due to an inability to accurately attend to threats in various environmental contexts. Previous literature and recent human imaging studies have demonstrated that PTSD patients often show LC hyperactivity (Liberzon and Abelson, 2016; McCall et al., 2015; Valentino and Van Bockstaele, 2008). Our study presented here supports the hypothesis that LC hyperactivity in PTSD patients may modulate hippocampal function and its association with contextual information processing potentially leading to context-related PTSD symptoms including hypervigilance. The current study provides a better understanding of the neuromodulatory mechanisms underlying fear discrimination and may help guide the development of unique therapeutic strategies using currently available noradrenergic ligands for targeting psychiatric disorders characterized by generalization such as is the case in PTSD, and schizophrenia (Lisman et al., 2008; Shohamy et al., 2010; Sammer et al., 2011).

STAR Methods

Resource Availability

Lead Contact—Further information and requests for resources and reagents should be directed to and will be fulfilled by the Lead Contact, Dr. Michael Bruchas (mbruchas@uw.edu).

Materials Availability—This study did not generate new or unique reagents or other materials.

Data and Code Availability—Custom MATLAB analysis code was created to appropriately organize, process, and combine imaging data with associated behavioral data. Analysis code for imaging from Figures 2 and 3 is available online at https://

www.github.com/BruchasLab. The full behavioral dataset supporting the current study are available from the corresponding author upon request.

Experimental Model and Subject Details

Animals—Adult (25-35 g) male *TH*-IRES-Cre mice, *Dbh*-Cre mice, *vGAT*-IRES-Cre mice, *vGlut1*-IRES-Cre mice, and Cre (−) littermate control mice were used for projection mapping and all *in vivo* experiments after backcrossing to C57BL/6J mice for at least 10 generations. Mice were group housed, given access to food pellets and water *ad libitum,* and maintained on a 12:12-hour light/dark cycle (lights on at 7:00 a.m.). Animals were held in a sound attenuated holding room facility in the lab starting at least one week prior to surgery, as well as post-surgery and throughout the duration of behavioral assays to minimize stress from transportation and disruption from foot traffic. All mice were handled and, where appropriate, connected to fiber optics and/or a miniscope two times a day for one week prior to behavioral experimental testing. All experimental procedures were approved by the Animal Care and Use Committee of Washington University and the Animal Care and Use Committee of University of Washington and conformed to NIH guidelines.

Method Details

Stereotaxic Surgery—All surgeries were performed under 4% isoflurane anesthesia (Piramal Healthcare, Maharashtra, India). For initial projection mapping, adult male mice were injected unilaterally with 800 nl of AAV5-EF1α-DIO-ChR2-eYFP virus (WUSTL Hope Center Viral Core, St. Louis, MO) into the LC (AP: −5.44 mm, ML: +1.25 mm, DV: −3.8 mm) using a Hamilton syringe with beveled needle (Reno, NV). For retrograde tracing, 300-400 nl of Cholera Toxin B (CTB), rAAV2-retro was injected into the DG (AP: −2.2 mm, ML: +1.4 mm, DV: −2.1) using a Hamilton syringe with blunted needle. For functional LC-DG necessity and sufficiency behavior experiments, adult male mice were injected bilaterally with 800 nl of AAV5-EF1α-DIO-ChR2-eYFP, or AAV5-EF1α-DIO-ArchT-eGFP virus (WUSTL Hope Center Viral Core, St. Louis, MO) into the LC (AP: −5.45 mm, ML: ±1.25 mm, DV: −3.8 mm) using a Hamilton syringe with a beveled needle. For transgenic controls, adult mice were injected bilaterally with 800 nl of AAV5-EF1α-DIO-eYFP into the LC (AP: −5.45 mm, ML: ±1.25 mm, DV: −3.8 mm) using a Hamilton syringe with a beveled needle. To stimulate DG cell types via β-adrenergic receptor signaling, 400 nl of the light sensitive chimeric rhodopsin/β_2-adrenergic receptor AAV5-EF1α-DIO-Opto-β_2AR-YFP was injected bilaterally into the DG (AP: −2.2 mm, ML: ±1.4 mm, DV: −2.1 mm) using a Hamilton syringe with blunted needle. Four to five weeks after virus injection, fiber optic ferrules were chronically implanted above the DG (AP: −2.2 mm, ML: ±1.4 mm, DV: −1.65 mm), and dental cement (Lang Dental, Wheeling, IL) was applied to hold the ferrules in place. For electrophysiological recordings, adult mice were injected bilaterally with 400 nl of AAV5-EF1α-DIO-eYFP into the DG (AP: −2.2 mm, ML: ±1.4mm, DV: −2.1 mm). Mice were allowed to recover for at least six weeks following infusion of virus prior to further behavioral testing or perfusion for projection mapping to ensure optimal viral expression and implant placement location (Fig. S2A).

For in vivo Ca^{2+} imaging experiments, we first tested several dilutions of AAV5-CaMKIIα-GCAMP6f (1.31x1013 VG/ml, 1:1,1:3,1:10) to ensure optimal expression within the DG

to ensure accurate sparse labeling for ideal imaging conditions (1:3). We then injected unilaterally with 400 nl of AAV5-CaMKIIα-GCAMP6f into the DG area (AP: −2.15, ML: +1.4, DV: −2.1) using a Hamilton syringe with blunted needle, and 800 nl of AAV5-Syn-DIO-HM3D(Gq)-mCherry into the LC using a Hamilton syringe with beveled needle. After waiting at least two weeks to allow for viral spread, we implanted a microendoscopic GRIN lens (1mm diameter x 4mm in length) 100 microns above the previously injected dorsal DG (AP: −2.15, ML: +1.4, DV: −2.0) using the previously described protocol (Resendez et al., 2016). Briefly, using a trephine drill bit, a circular portion of the skull was removed from above the viral injection site and exposed tissue was washed with saline. The GRIN lens was then slowly lowered (100μm/min) into place with a stable stereotaxic holder attachment. Superglue was used to fix the lens in place and prevent movement during imaging, and a dental cement wall was built on the skull surrounding the lens with 2-3 anchor screws inserted into surrounding areas of the skull for support. The lens was then covered with silicone elastomer sealant (Kwik-Cast) for 1-2 weeks before checking for visibly fluorescent cells. Once the best focus was obtained, a baseplate (Inscopix) was mounted with superglue on top of the skullcap, surrounding the lens at the optimal focal distance for imaging. To acclimate the mice to the weight of the microscope, a dummy scope weighing 2g was attached to the baseplate when not using the microscope for imaging. Mice were perfused at the conclusion of behavior to ensure optimal viral expression and implant placement location (Fig. S3A, I).

Tissue Collection and Immunohistochemistry—After the conclusion of behavioral testing, mice were anesthetized with sodium pentobarbital and transcardially perfused with ice-cold PBS, followed by 4% phosphate-buffered paraformaldehyde. Brains were removed, postfixed overnight in 4% paraformaldehyde, and then saturated in 30% phosphate-buffered sucrose for 2-4 days at 4°C. The brain tissue was flash-frozen and sectioned coronally at 35 μm thickness on a microtome.

For immunofluorescence labeling, sections were incubated in blocking solution (PBS with 5% normal donkey serum and 0.25% Triton X-100) for 1 hour with gentle agitation before incubation with primary antibodies: rabbit anti-GAD65/67 (1:1000) and anti-GAD65 (1:1000, Millipore Cat# AB1511, RRID: AB_11210186), chicken anti-TH (1:1000, Aves Labs). Sections were incubated with primary antibodies at room temperature overnight and rinsed for 5 minutes in 3 changes of PBS. Secondary antibodies (Alexa Fluor 568-conjugated goat anti-rabbit, Alexa Fluor 568-conjugated goat anti-chicken, Alexa Fluor 633-conjugated goat anti-chicken, Invitrogen) were diluted in PBS (secondary antibodies at 1:1000) with 5% normal goat serum and 0.25% Triton X-100. Sections were incubated for 2 hours at room temperature with gentle agitation and then rinsed in PBS, mounted, and cover slipped with/without DAPI. YFP labeled cells were pseudocolored as green.

Viral ChR2 expression was verified using fluorescence and confocal (Leica Microsystems) microscopy. Images were produced with 10X, 20X, 63X objective and analyzed using ImageJ software (NIH) and Leica Application Suite Advanced Fluorescence software. For the counting of ChR2-expressing LC-NE axons in the hippocampus, three brain sections from each animal were selected (From Bregma −1.46, −1.82, −2.30). The 250 x 250 μm squared area in each subregion in both right and left hemi-spares were selected (i.e. in the

center of the DG, CA3, and CA; Fig. 1A), and then manually counted the number of eGFP positive axons within the area, averaged all six values from three sections, treated as a value of a subject, and then converted to mm^2 unit.

Quantification of viral transfection of Opto-β_2 in DG hilus and GCL was done using Halo Image Analysis Software (Indica Labs). Using slide images taken using a confocal microscope, borders were set to delineate DG hilus and GCL. Then, the overlap in fluorescent signal between DAPI and Opto-β_2-eYFP was analyzed and reported for hilus and GCL in vGlut1-Cre and vGAT-Cre mice (Fig. S4F-G).

Fear Conditioning—Fear conditioning took place in Med-Associates conditioning chambers that consisted of one clear plexiglass wall, three aluminum walls, and a stainless steel grid as a floor. The training chamber was housed in a sound attenuated cubicle. The conditioning chambers could be configured into three distinct contexts: A, B, and C. Context A was rectangular, with floors made of stainless steel rods (2 mm diameter, spaced 5 mm apart), walls of aluminum and acrylic, and cinnamon extract scent, and was cleaned with 70% ethanol between runs. Context B differed from context A in that it had a white acrylic floor and a wall decorated with a black and white striped pattern. Context B was cleaned with multi-purpose surface cleaner (Method, UPC: 817939000106) between runs, and scented with peppermint extract. Context C also had a white acrylic floor, however it differed from context B in that the chamber walls were covered with circular plastic inserts, and the cubicle fan was turned off. Context C was cleaned with multi-purpose surface cleaner (Method, UPC: 817939000106) between runs, and scented with peppermint extract. All sessions were recorded from the side using a digital camera and were scored for freezing by an investigator blind to the genotype of the animal.

For optogenetic controls during behavior tests, a rotating optical commutator (Doric) was positioned on top of the training chamber and connected to a 473 nm or 543 nm diode-pumped solid-state laser (OEM Laser Systems; see Fig. 1A, 1F, 4F, 4L). Fibers were attached to the implants on the mouse for every training session. Laser power was adjusted to obtain ~15 mW transmittance into the brain.

Contextual Fear Discrimination (CFD)—Mice were handled for 5 minutes per day for a week prior to training. Contextual fear discrimination training took place in the apparatus described above. In context A (unsafe context), animals were placed in the conditioning chamber and allowed to freely explore for 180 seconds, after which they received a single 2 second foot shock of 0.50 mA. Mice were taken out 15 seconds after termination of the foot shock and returned to their home cage. In context B (safe context), mice were allowed to freely explore the context for 197 seconds, the same amount of total time that they were in context A, and then returned to their home cage. In this context, no foot shock was delivered. All freezing in both contexts was assessed for the first 180 seconds, and the last 17 seconds were not included in the behavioral analysis. Freezing was done in a double-blind fashion to avoid bias in manual scoring.

On the first day (Day 0) of CFD training, all animals were placed in context A and received a foot shock. The next day (Day 1), for LC-DG activation (Fig. 1D), imaging experiments

(Fig. 2C, Fig. 3C), propranolol experiment (Fig. 4C), and opto-B2 modulation (Fig. 4I) experiments, mice were run first in context B with no foot shock, then in context A with a foot shock. There was a minimum 3 hour period between exposure to context A and context B. This training protocol was repeated daily for 9 days. For the LC-DG inhibition (Fig. 1G) experiment, the order of the exposed contexts (A and B) during training was randomized to make the training more challenging. For the discrimination training (Fig. S1M, Fig. S1P), the training procedure followed the same schedule as the LC-DG activation or inhibition experiments, with context C (dissimilar context) replacing context B.

For the stress-modulated CFD training (Fig. 4S-U), mice were immobilized in modified disposable conical tubes once for 5 minutes and were then immediately transferred to their home cages. Animals were subjected to CFD as described above. To evaluate whether the stress-induced behavioral outcome was due to the cognitive impairment or changes in pain sensitivity, the unconditioned response to foot shock was assessed by estimating horizontal distance traveled during the shock. Horizontal distance was estimated by quantifying crossings of a 4-cell grid superimposed over the conditioning chamber (Fig. S1K). When conducting *in vivo* imaging during CFD (Fig. 2C, 3C), mice were injected with CNO (5 mg/kg, i.p., 30 minutes prior) before CFD training. For transgenic controls, mice were injected with saline instead of CNO i.p. 30 minutes prior to CFD training. When conducting β-AR loss of function experiment (Fig. 4C), mice were injected with either saline or Propranolol (10 mg/kg, i.p., 1 hour prior) followed by CNO (5 mg/kg, i.p., 30 minutes prior) before CFD training.

RNAscope Fluorescence In Situ Hybridization (FISH)—Following rapid decapitation of mice, brains were flash frozen in −50°C 2-methylbutane and stored at −80°C for further processing. Coronal sections containing hippocampal regions that corresponded to the injection plane used in the behavioral experiments were cut at 20 μm at −20°C and thaw-mounted onto Super Frost Plus slides (Fisher). Slides were stored at −80°C until further processing. FISH was performed according to the RNAScope® 2.0 Fluorescent Multiple Kit User Manual for Fresh Frozen Tissue (Advanced Cell Diagnostics, Inc.) (Wang et al., 2012). Slides containing the specified coronal brain sections were fixed in 4% paraformaldehyde, dehydrated, and pretreated with protease IV solution for 30 minutes. Sections were then incubated for target probes for mouse *PNOC*, (accession number NM_010932.2, probe region 325-1263), *Vglut1* (*slc17a7*, accession number NM_182993.2, probe region 464-1415), *Vglut2* (*slc17a6*, accession number NM_080853.3, probe region 1986-2998), *Vglut3* (*slc17a8*, accession number NM_182959.3, probe region 781-1695), *Vgat* (*slc32a1*, accession number NM_009508.2, probe region 894-2037), and *Adrb2* (*slc17a8*, accession number NM_007420.3, probe region 55-962) for 2 hrs. All target probes consisted of 20 ZZ oligonucleotides and were obtained from Advanced Cell Diagnostics. Following probe hybridization, sections underwent a series of probe signal amplification steps (AMP1-4) including a final incubation of fluorescently labeled probes (Alexa 488, Atto 550, Atto 647), designed to target the specified channel (C1-C3 depending on assay) associated with the probes. Slides were counterstained with DAPI and coverslips were mounted with Vectashield Hard Set mounting medium (Vector Laboratories). Images were obtained on a Leica TCS SPE confocal microscope (Leica), and Application Suite Advanced

Fluorescence (LAS AF) software was used for analyses. For each cell, the total pixels of fluorescent signal were counted, with the assumption that each pixel represented a single molecule of RNA. Selection criterion was set to 10 total positive pixels after adjusting threshold with ImageJ software. Since the clustering morphology of cells within the dentate gyrus does not allow for a clear interpretation for what constitutes a positive cell, only the hilus was used for quantification.

Open Field Test (OFT)—OFT testing was performed in a custom-made white box (50 cm X 50 cm) within a sound-attenuated room maintained at_23°C. The 'center' area was defined as a square of 50% the total OFT area. A light bulb mounted above provided 45 lux illumination, measured in the center of the arena. Mice were handled for 5 minutes per day for a week prior to the OFT testing. On the day of OFT testing, mice were habituated in a holding room for 30 minutes and then they were allowed to explore the entire chamber freely for 25 min. Sessions were recorded via a digital camera, and videos were analyzed off-line using Ethovision XT 8.5 (Noldus Information Technologies). The open field was cleaned with 70% ethanol between each trial. Ethovision XT 8.5 (Noldus Information Technologies) quantified the total distance and time spent in the central and peripheral areas. Time spent in the center of the open field was used as a measure of anxiolysis.

Slice Preparation—Coronal brain slices were prepared at 250 μM on a vibrating Leica VT1000S microtome using standard procedures. Mice were anesthetized with Euthasol (Virbac, Westlake Texas), and transcardially perfused with ice-cold and oxygenated cutting solution consisting of (in mM): 93 N-Methyl-D-glucamine (NMDG), 2.5 KCL, 20 HEPES, 10 MgSO4·7H20, 1.2 NaH2PO4, 0.5 CaCl2·2H20, 25 glucose, 3 Na^+-pyruvate, 5 Na^+-ascorbate, and 5 N-acetylcysteine. Following collection of coronal sections, the brain slices were transferred to a 34°C chamber containing oxygenated cutting solution for a 10-minute recovery period. Slices were then transferred to a holding chamber consisting of (in mM) 92 NaCl, 2.5 KCl, 20 HEPES, 2 MgSO4·7H20, 1.2 NaH2PO4, 30NaHCO3, 2 CaCl2·2H20, 25 glucose, 3 Na-pyruvate, 5 Na-ascorbate, 5 N-acetylcysteine and were allowed to recover for ≥ 30 min. For recording, slices were perfused with oxygenated artificial cerebrospinal fluid (ACSF; 31-33°C) consisting of (in mM): 113 NaCl, 2.5 KCl, 1.2 MgSO4·7H20, 2.5 CaCl2·6H20, 1 NaH2PO4, 26 NaHCO3, 20 glucose, 3 Na^+-pyruvate, 1 Na^+-ascorbate, at a flow rate of 2-3ml/min. 50mM Propranolol Hydrochloride and 5mM Isoproterenol Hydrochloride was made fresh each day in ddH_2O and added to either the HEPES or ACSF in a 1:1000 ratio for a final concentration of 50μM and 5μM, respectively.

Fluorescently labeled VGAT+ neurons in the DG were identified using a Thorlabs LEDD1B T-Cube driver at 40x magnification with an immersion objective with differential interference contrast (DIC) microscopy. DG neurons were initially voltage clamped in whole-cell configuration using borosilicate glass pipettes (2-4MΩ). filled with internal solution containing (in mM): 125 K^+-gluconate, 4 NaCl, 10 HEPES, 4 MgATP, 0.3 Na-GTP, and 10 Naphosphocreatine (pH 7.30-7.35). For all experiments, neurons were clamped at −70mV and 50 μM picrotoxin (Cayman Chemical, Ann Arbor, Michigan) was included in the patch pipette. Following break-in to the cell, we waited ≥ 3 minutes to allow for exchange of internal solution and stabilization of membrane properties. Neurons with an

access resistance of > 30MΩ or that exhibited greater than a 20% change in access resistance during the recording were not included in our datasets. After allowing the neurons to stabilize following break in, they were switched into current-clamp mode for the collection of the data presented in figure 4. Cells that showed spontaneous firing activity or fired prior to depolarization steps were excluded from the data set.

***In Vivo* Ca^{2+} Imaging Data Processing—**nVista acquisition software (Inscopix) was used to acquire images of fluorescence dynamics at 20 frames per second. Fear conditioning control software Video Freeze (Med Associates) was programmed to trigger the beginning of the imaging session with recording of fear behavior simultaneously.

Mosaic (Inscopix) was used to preprocess Ca^{2+} data from each imaging session as previously described (Resendez et al., 2016; Jennings et al., 2015; Rubin et al., 2015; Ziv et al., 2013). Briefly, for each day, calcium imaging data from context A and context B were down-sampled temporally (2x temporal bin) and spatially (2x spatial bin), concatenated together, and rigid motion correction was applied. After preprocessing, putative single neuron activity was segmented using Constrained Non-negative Matrix Factorization for Endoscopic data (CNMFe) according to established criteria using custom MATLAB (MathWorks, Natick, MA, USA) scripts and sorted manually by a blind observer according to established criteria (Resendez et al., 2016; Zhou et al., 2018). Background components were estimated using the “ring” model, which was chosen after thorough parametrization to limit the presence of non-neuronal signals in our dataset.

Following sorting, individual putative single neurons were tracked between Days 1 and 9 during the CFD task using CellReg (Sheintuch et al., 2017). For each mouse the spatial correlation registration threshold performed best, and optimal correlation thresholds were determined by the algorithm. Final registration utilized the probabilistic model for all mice.

Following sorting, individual putative single neurons were tracked between Days 1 and 9 during the CFD task using CellReg (PMID: 29069591; Sheintuch et al., 2017). For each mouse the spatial correlation registration threshold performed best, and thresholds were determined by the algorithm. Final registration utilized the probabilistic model for all mice.

To assess the link between cell selectivity and behavior in the CFD task, a Pearson correlation was conducted for Days 1 and 9 for Th-$Cre^{LC\text{-}DG}$::HM3Dq mice as well as wild-type controls (Fig. 2M, Fig. 3I). This Pearson correlation utilized the ratio of cells selective to context A vs. context B compared to the ratio of freezing in context B vs. context A.

To assess changes in ensemble activity over the course of training, we examined neurons classified on day 9 as either responding selectively to context A, context B, or nonselectively as a subset of selectivity on day 1 (Fig. 2P, Fig. 3K). This produced nine subsets of neuron activity: percentage of neurons responsive to A on both days, responsive to A on day 1 and B on day 9, responsive to A on day 1 and nonselective on day 9, etc.

***In Vivo* Ca^{2+} Imaging Data Analysis—**Raw fluorescence traces for individual putative neurons were Z-normalized ($Z = \frac{x - \mu}{\sigma}$) to their session average activity for Day 1 and Day 9 using custom MATLAB code. In order to classify cells as selective for context A, context B, or non-selective, a two-tailed t-test comparing event traces during the first 180 seconds (1800 samples) in context A to the subsequent 180 seconds (1800 samples) in context B for each day (Fig. S3H). A critical $\alpha \leq 0.05$ was chosen to determine whether a cell was significantly more active in a specific context on a given day. Differences in context specific cell selectivity across training were determined using a chi-squared test.

Quantification and Statistical Analysis

All data are expressed as mean ± SEM. Behavioral data were analyzed with JMP12 Pro (SAS institute, Cary, NC, RRID:SCR_014242) and GraphPad Prism 8.0. *Student's t*-test, one-way or two-way ANOVAs were used to analyze between-subjects designs. Chi-squared tests (Jimenez et al., 2018; Jimenez et al., 2020) and Kolmogorov–Smirnov tests were used to analyze probability distributions. Repeated-measures designs were analyzed using mixed-effects restricted maximum likelihood (REML) model. Tukey was used for *post-hoc* pairwise comparisons. The null hypothesis was rejected at the $p < 0.05$ level. Statistical significance was taken as $*p < 0.05$, $**p < 0.01$, $***p < 0.005$, *n.s.* represents not significant. All statistical information is listed in Table S1.

Supplementary Material

Refer to Web version on PubMed Central for supplementary material.

Acknowledgments

Funding: This work was supported by National Institute of Health Grants: NIH R01MH112355, and BRAIN Initiative 1U01 MH10913301, and NIH P30DA048736, and R01 DA033396-04S1 (NIDA Diversity Supplement). We also thank Inscopix for the DECODE Award, which partially supported this work.

References and Notes:

Liberzon I, and Abelson JL (2016). Context Processing and the Neurobiology of Post-Traumatic Stress Disorder. Neuron 92, 14–30. [PubMed: 27710783]

Siegmund A, and Wotjak CT (2006). Toward an Animal Model of Posttraumatic Stress Disorder. Ann. N. Y. Acad. Sci 1071, 324–334. [PubMed: 16891581]

Hennings AC, McClay M, Lewis-Peacock JA, and Dunsmoor JE (2020). Contextual reinstatement promotes extinction generalization in healthy adults but not PTSD. Neuropsychologia. 147, 107573. [PubMed: 32735802]

Kheirbek MA, Klemenhagen KC, Sahay A, and Hen R (2012). Neurogenesis and Generalization: A New Approach to Stratify and Treat Anxiety Disorders. Nat. Neurosci 15, 1613–1620. [PubMed: 23187693]

Besnard A, and Sahay A (2016). Adult Hippocampal Neurogenesis, Fear Generalization, and Stress. Neuropsychopharmacology 41, 24–44. [PubMed: 26068726]

Morris RG (2006). Elements of a Neurobiological Theory of Hippocampal Function: The Role of Synaptic Plasticity, Synaptic Tagging and Schemas. Eur. J. Neurosci 23, 2829–2846. [PubMed: 16819972]

Lisman J, Buzsáki G, Eichenbaum H, Nadel L, Ranganath C, and Redish AD (2017). Viewpoints: How the Hippocampus Contributes to Memory, Navigation and Cognition. Nat. Neurosci 20, 1434–1447. [PubMed: 29073641]

O'Reilly RC, and McClelland JL (1994). Hippocampal Conjunctive Encoding, Storage, and Recall: Avoiding a Trade-Off. Hippocampus 4, 661–682. [PubMed: 7704110]

Treves A, Tashiro A, Witter MP, and Moser EI (2008). What Is the Mammalian Dentate Gyrus Good For? Neuroscience 154, 1155–1172. [PubMed: 18554812]

McHugh TJ, Jones MW, Quinn JJ, Balthasar N, Coppari R, Elmquist JK, Lowell BB, Fanselow MS, Wilson MA, and Tonegawa S (2007). Dentate Gyrus NMDA Receptors Mediate Rapid Pattern Separation in the Hippocampal Network. Science 317, 94–99. [PubMed: 17556551]

Deng W, Mayford M, and Gage FH (2013). Selection of Distinct Populations of Dentate Granule Cells in Response to Inputs as a Mechanism for Pattern Separation in Mice. Elife 2, e00312. [PubMed: 23538967]

Nakazawa K, Quirk MC, Chitwood RA, Watanabe M, Yeckel MF, Sun LD, Kato A, Carr CA, Johnston D, Wilson MA, et al. (2002). Requirement for Hippocampal CA3 NMDA Receptors in Associative Memory Recall. Science 297, 211–218. [PubMed: 12040087]

Marr D (1971). Simple Memory: A Theory for Archicortex. Philos. Trans. R. Soc. Lond. B. Biol. Sci 262, 23–81. [PubMed: 4399412]

Blackstad TW, Fuxe K, and Hökfelt T (1967). Noradrenaline Nerve Terminals in the Hippocampal Region of the Rat and the Guinea Pig. Z. Zellforsch Mikrosk Anat 78, 463–473. [PubMed: 5598548]

McCall JG, Al-Hasani R, Siuda ER, Hong DY, Norris AJ, Ford CP, and Bruchas MR (2015). CRH Engagement of the Locus Coeruleus Noradrenergic System Mediates Stress-Induced Anxiety. Neuron 87, 605–620. [PubMed: 26212712]

Valentino RJ, and Van Bockstaele E (2008). Convergent Regulation of Locus Coeruleus Activity as an Adaptive Response to Stress. Eur. J. Pharmacol 583, 194–203. [PubMed: 18255055]

Harley CW (2007). Norepinephrine and the Dentate Gyrus. Prog. Brain. Res 163, 299–318. [PubMed: 17765726]

Walling SG, and Harley CW (2004). Locus Ceruleus Activation Initiates Delayed Synaptic Potentiation of Perforant Path Input to the Dentate Gyrus in Awake Rats: A Novel Beta-Adrenergic- And Protein Synthesis-Dependent Mammalian Plasticity Mechanism. J. Neurosci 24, 598–604. [PubMed: 14736844]

Seidenbecher T, Reymann KG, and Balschun D (1997). A Post-Tetanic Time Window for the Reinforcement of Long-Term Potentiation by Appetitive and Aversive Stimuli. Proc. Natl. Acad. Sci. U S A 94, 1494–1499. [PubMed: 9037081]

Rose GM, and Pang KC (1989). Differential Effect of Norepinephrine Upon Granule Cells and Interneurons in the Dentate Gyrus. Brain Res. 488, 353–356. [PubMed: 2743131]

Lovett-Barron M, Kaifosh P, Kheirbek MA, Danielson N, Zaremba JD, Reardon TR, Turi GF, Hen R, Zemelman BV, and Losonczy A (2014). Dendritic Inhibition in the Hippocampus Supports Fear Learning. Science 343, 857–863. [PubMed: 24558155]

Danielson NB, Kaifosh P, Zaremba JD, Lovett-Barron M, Tsai J, Denny CA, Balough EM, Goldberg AR, Drew LJ, Hen R, et al. (2016). Distinct Contribution of Adult-Born Hippocampal Granule Cells to Context Encoding. Neuron 90, 101–112. [PubMed: 26971949]

Tervo DG, Hwang BY, Viswanathan S, Gaj T, Lavzin M, Ritola KD, Lindo S, Michael S, Kuleshova E, Ojala D, et al. (2016). A Designer AAV Variant Permits Efficient Retrograde Access to Projection Neurons. Neuron 92, 372–382. [PubMed: 27720486]

Han X, Chow BY, Zhou H, Klapoetke NC, Chuong A, Rajimehr R, Yang A, Baratta MV, Winkle J, Desimone R, et al. (2011). A High-Light Sensitivity Optical Neural Silencer: Development and Application to Optogenetic Control of Non-Human Primate Cortex. Front. Syst. Neuro 5, 18.

Sara SJ (2009). The Locus Coeruleus and Noradrenergic Modulation of Cognition. Nat. Rev. Neurosci 10, 211–223. [PubMed: 19190638]

Mair RD, Zhang Y, Bailey KR, Toupin MM, and Mair RG (2005). Effects of Clonidine in the Locus Coeruleus on Prefrontal- And Hippocampal-Dependent Measures of Attention and Memory in the Rat. Psychopharmacology (Berl.) 181, 280–288. [PubMed: 15830223]

Kempadoo KA, Mosharov EV, Choi SJ, Sulzer D, and Kandel ER (2016). Dopamine Release From the Locus Coeruleus to the Dorsal Hippocampus Promotes Spatial Learning and Memory. Proc. Natl. Acad. Sci. U S A. 113, 14835–14840. [PubMed: 27930324]

Takeuchi T, Duszkiewicz AJ, Sonneborn A, Spooner PA, Yamasaki M, Watanabe M, Smith CC, Fernández G, Deisseroth K, Greene RW, et al. (2016). Locus Coeruleus and Dopaminergic Consolidation of Everyday Memory. Nature 537, 357–362. [PubMed: 27602521]

Hagena H, Hansen N, and Manahan-Vaughan D β-Adrenergic Control of Hippocampal Function: Subserving the Choreography of Synaptic Information Storage and Memory. Cereb. Cortex 26, 1349–1364.

Lethbridge RL, Walling SG, and Harley CW (2014). Modulation of the perforant path-evoked potential in dentate gyrus as a function of intrahippocampal β-adrenoceptor agonist concentration in urethane-anesthetized rat. Brain Behav. 4, 95–103. [PubMed: 24653959]

Seo DO, and Bruchas MR (2017). Polymorphic Computation in Locus Coeruleus Networks. Nat. Neurosci 20, 1517–1519. [PubMed: 29073646]

Wagatsuma A, Okuyama T, Sun C, Smith LM, Abe K, and Tonegawa S (2018). Locus Coeruleus Input to Hippocampal CA3 Drives Single-Trial Learning of a Novel Context. Proc. Natl. Acad. Sci. U S A. 115, E310–E316. [PubMed: 29279390]

Siuda ER, McCall JG, Al-Hasani R, Shin G, Il Park S, Schmidt MJ, Anderson SL, Planer WJ, Rogers JA, and Bruchas MR (2015). Optodynamic Simulation of β-adrenergic Receptor Signalling. Nat. Commun 6, 8480. [PubMed: 26412387]

Houser CR (2007). Interneurons of the Dentate Gyrus: An Overview of Cell Types, Terminal Fields and Neurochemical Identity. Prog. Brain. Res 163, 217–232. [PubMed: 17765721]

Stadel JM, Lefkowitz RJ (1991). The Beta-Adrenergic Receptors. The Receptors 1, 1–40.

Arnsten AF (2011). The use of α-2A adrenergic agonists for the treatment of attention deficit/hyperactivity disorder. Expert Rev. Neurother 10, 1595–1605.

Franowicz JS, Kessler LE, Dailey Borja CM, Kobilka BK, Limbird LE, and Arnsten AF (2002). Mutation of the alpha2A-adrenoceptor impairs working memory performance and annuls cognitive enhancement by guanfacine. J. Neurosci. 22, 8771–8777. [PubMed: 12351753]

Arnsten AF (2009) Stress signalling pathways that impair prefrontal cortex structure and function. Nat. Rev. Neurosci 10, 410–422 [PubMed: 19455173]

Berridge CW and Spencer RC (2016). Differential cognitive actions of norepinephrine a2 and a1 receptor signaling in the prefrontal cortex. Brain Res. 1641, 189–196. [PubMed: 26592951]

Kaouane N, Porte Y, Vallée M, Brayda-Bruno L, Mons N, Calandreau L, Marighetto A, Piazza PV, and Desmedt A (2012). Glucocorticoids Can Induce PTSD-like Memory Impairments in Mice. Science 335, 1510–1513. [PubMed: 22362879]

Uematsu A, Tan BZ, Ycu EA, Cuevas JS, Koivumaa J, Junyent F, Kremer EJ, Witten IB, Deisseroth K, and Johansen JP (2017). Modular Organization of the Brainstem Noradrenaline System Coordinates Opposing Learning States. Nat. Neurosci 20, 1602–1611. [PubMed: 28920933]

Pang K, and Rose GM (1987). Differential effects of norepinephrine on hippocampal complex-spike and theta-neurons. Brain Res. 425, 146–158. [PubMed: 2892569]

Milner TA, Shah P, and Pierce JP (2000). beta-adrenergic receptors primarily are located on the dendrites of granule cells and interneurons but also are found on astrocytes and a few presynaptic profiles in the rat dentate gyrus. Synapse 36, 178–193. [PubMed: 10819898]

Cox DJ, Racca C, and LeBeau FE (2008). Beta-adrenergic receptors are differentially expressed in distinct interneuron subtypes in the rat hippocampus. J. Comp. Neurol 509, 551–565. [PubMed: 18546278]

Kaufman AM, Geiller T, and Losonczy A (2020). A Role for the Locus Coeruleus in Hippocampal CA1 Place Cell Reorganization during Spatial Reward Learning. Neuron 105, 1018–1026. [PubMed: 31980319]

Feng J, Zhang C, Lischinsky JE, Jing M, Zhou J, Wang H, Zhang Y, Dong A, Wu Z, Wu H, Chen W, Zhang P, Zou J, Hires SA, Zhu JJ, Cui G, Lin D, Du J, and Li Y (2019). A Genetically Encoded Fluorescent Sensor for Rapid and Specific In Vivo Detection of Norepinephrine. Neuron 102, 745–761. [PubMed: 30922875]

Gazarini L, Jark Stern CA, Carobrez AP, and Bertoglio LJ (2013). Enhanced noradrenergic activity potentiates fear memory consolidation and reconsolidation by differentially recruiting α1- and β-adrenergic receptors. Learn. Mem. 20, 210–219. [PubMed: 23512937]

Otis JM, Werner CT, and Mueller D (2015). Noradrenergic regulation of fear and drug-associated memory reconsolidation. Neuropsychopharmacology 40, 793–803. [PubMed: 25315025]

Raimondo JV, Kay L, Ellender TJ, Akerman CJ (2012). Optogenetic silencing strategies differ in their effects on inhibitory synaptic transmission. Nat. Neurosci 15, 1102–1104. [PubMed: 22729174]

Mahn M, Prigge M, Ron S, Levy R, and Yizhar O (2016). Biophysical constraints of optogenetic inhibition at presynaptic terminals. Nat. Neurosci 19, 554–556. [PubMed: 26950004]

Lissek S, Rabin S, Heller RE, Lukenbaugh D, Geraci M, Pine DS, and Grillon C (2010). Overgeneralization of Conditioned Fear as a Pathogenic Marker of Panic Disorder. Am. J. Psychiatry 167, 47–55. [PubMed: 19917595]

Lisman JE, Coyle JT, Green RW, Javitt DC, Benes FM, Heckers S, and Grace AA (2008). Circuit-based framework for understanding neurotransmitter and risk gene interactions in schizophrenia. Trends Neurosci. 31, 234–242. [PubMed: 18395805]

Shohamy D, Mihalakos P, Chin R, Thomas B, Wagner AD, and Tamminga C (2010). Learning and Generalization in Schizophrenia: Effects of Disease and Antipsychotic Drug Treatment. Biol. Psychiatry 67, 926–932. [PubMed: 20034612]

Sammer G, Leifheit S, Dettbarn A, and Gallhofer B (2011). Effects of context information on emotion recognition in schizophrenia. International Clinical Psychopharmacology 26, e175.

Resendez SL, Jennings JH, Ung RL, Namboodiri VM, Zhou ZC, Otis JM, Nomura H, McHenry JA, Kosyk O, and Stuber GD (2016). Visualization of Cortical, Subcortical and Deep Brain Neural Circuit Dynamics During Naturalistic Mammalian Behavior With Head-Mounted Microscopes and Chronically Implanted Lenses. Nat. Protoc 11, 566–597. [PubMed: 26914316]

Wang F, Flanagan J, Su N, Wang LC, Bui S, Nielson A, Wu X, Vo HT, Ma XJ, and Luo Y (2012). RNAscope: A Novel in Situ RNA Analysis Platform for Formalin-Fixed, Paraffin-Embedded Tissues. J. Mol. Diagn 14, 22–29. [PubMed: 22166544]

Jennings JH, Ung RL, Resendez SL, Stamatakis AM, Taylor JG, Huang J, Veleta K, Kantak PA, Aita M, Shilling-Scrivo K, et al. (2015). Visualizing Hypothalamic Network Dynamics for Appetitive and Consummatory Behaviors. Cell 160, 516–527. [PubMed: 25635459]

Rubin A, Geva N, Sheintuch L, and Ziv Y (2015). Hippocampal Ensemble Dynamics Timestamp Events in Long-Term Memory. Elife 4, e12247. [PubMed: 26682652]

Sheintuch L, Rubin A, Brande-Eilat N, Geva N, Sadeh N, Pinchasof O, and Ziv Y (2017). Tracking the Same Neurons across Multiple Days in Ca^{2+} Imaging Data. Cell Rep. 21, 1102–1115. [PubMed: 29069591]

Zhou P, Resendez SL, Rodriguez-Romaguera J, Jimenez JC, Neufeld SQ, Giovannucci A, Friedrich J, Pnevmatikakis EA, Stuber GD, Hen R, Kheirbek MA, et al. (2018). Efficient and Accurate Extraction of in Vivo Calcium Signals From Microendoscopic Video Data. Elife 7, e28728. [PubMed: 29469809]

Jimenez JC, Su K, Goldberg AR, Luna VM, Biane JS, Ordek G, Zhou P, Ong SK, Wright MA, Zweifel L, et al. (2018). Anxiety Cells in a Hippocampal-Hypothalamic Circuit. Neuron 97, 670–683. [PubMed: 29397273]

Jimenez JC, Berry JE, Lim SC, Ong SK, Kheirbek MA, and Hen R (2020). Nat. Commun 11, 3492. [PubMed: 32661319]

Highlights

- Bidirectional manipulation of LC^{NE}-DG circuits alters aversive contextual learning
- DG neuronal ensembles shift context selectivity during aversive contextual conditioning
- Chemogenetic LC^{NE} excitation during conditioning impairs DG ensemble dynamics
- β-adrenergic and GABA hilar interneuron modulation disrupt contextual learning

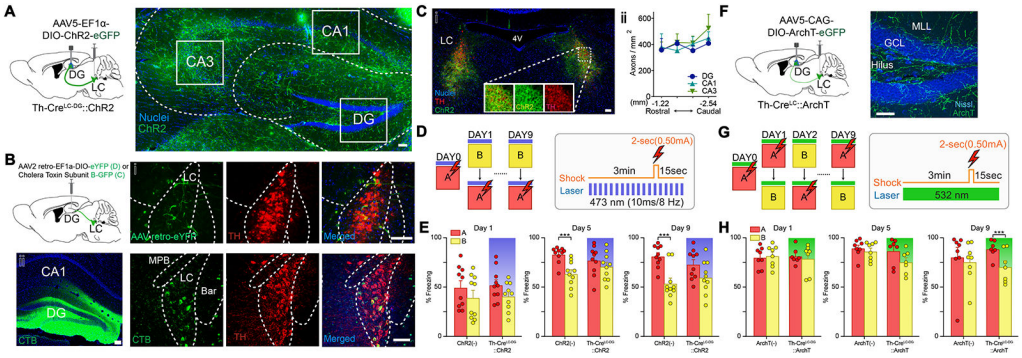

Fig. 1. Optogenetic manipulation of the LC-DG circuit in contextual fear discrimination.

(**A**) Schematic of experimental approach depicts infection of locus coeruleus-norepinephrine (LC-NE) cells using Th-Cre mouse line with channelrhodopsin (Th-Cre$^{LC\text{-}DG}$::ChR2). ChR2^{+} fibers indicate axons in the dorsal hippocampus originating from the TH^{+}-LC cells. Scale bar = 50 μm. (**B**) Retrograde tracing from the DG using Retro-AAV (top) or Green-CTB (bottom). Arrows indicate cells projecting to the DG that coexpress with TH. Scale bars = 100 μm. (**C**) ChR2-expressing LC-NE cells coexpressed tyrosine hydroxylase (TH). Scale bar = 100 μm. The density of ChR2^{+} fibers in the DG in hippocampal subregions: dentate gyrus (DG), CA1, and CA3. (**D**) CFD task with optogenetic activation of the LC-DG projection. Animals received a shock in context A (red), but not in context B (yellow) for nine days (left). Pattern of laser stimulation and shock (only in context A) during CFD (right). (**E**) Acute activation of the LC-DG projection impairs behavioral pattern separation in mice expressing ChR2 in LC-DG projections (Th-Cre$^{LC\text{-}DG}$::ChR2, n = 10), but not in wild-type controls (ChR2(−), n = 10). ChR2(−) controls were able to discriminate on the fifth and ninth days of training, while Th-Cre$^{LC\text{-}DG}$::ChR2 could not discriminate on those days (ChR2(−): Day 1A: 49.8 ± 6.61; Day 1B: 39.6 ± 6.99; Day 5A: 83.2 ± 2.54; Day 5B: 63.7 ± 4.08; Day 9A: 81.6 ± 3.51; Day 9B: 53.9 ± 5.23; Th-Cre$^{LC\text{-}DG}$::ChR2: Day 1A: 52.4 ± 5.14; Day 1B: 40.8 ± 4.48; Day 5A: 77.2 ± 4.64; Day 5B: 70.9 ± 4.36; Day 9A: 73.2 ± 4.68; Day 9B: 59.8 ± 5.42; Two-way ANOVA for Th-Cre$^{LC\text{-}DG}$::ChR2 vs ChR2(−), A vs B: Day 1: Group: $F_{(1,18)} = 0.055$, $p = 0.818$; Context: $F_{(1,18)} = 16.885$, $p < 0.001$; Group × Context: $F_{(1,18)} = 0.076$, $p = 0.786$; Day 5: Group: $F_{(1,18)} = 0.012$, $p = 0.913$; Context: $F_{(1,18)} = 30.608$, $p < 0.001$; Group × Context: $F_{(1,18)} = 8.034$, $p = 0.011$; Day 9: Group: $F_{(1,18)} = 0.040$, $p = 0.843$; Context: $F_{(1,18)} = 36.016$, $p < 0.001$; Group × Context: $F_{(1,18)} = 4.463$, $p = 0.049$). Both groups received optogenetic light during trial, shaded bar denotes successful stimulation of opsin. (**F**) Schematic of experimental approach depicts infection of LC-NE cells using Th-Cre mouse line with archaerhodopsin (Th-Cre$^{LC\text{-}DG}$::ArchT). Expression of ArchT in the DG regions (right). Scale bar = 50 μm. (**G**) CFD task with optogenetic inhibition of the LC-DG projection. Animals received a shock in context A (red), but not in context B (yellow) for nine days (left). Pattern of laser stimulation and shock (only in context A) during a CFD session (right). (**H**) Acute inhibition of LC-DG projection resulted in enhancement of behavioral pattern separation in mice expressing ArchT in LC-DG projections (Th-Cre$^{LC\text{-}DG}$::ArchT, n = 8), but not in wild-type controls (ArchT(−), n = 8). Th-Cre$^{LC\text{-}DG}$::ArchT animals were able to discriminate on the ninth day of training, while ArchT(−) controls could not discriminate on those days (ArchT(−): Day 1A: 80.3 ± 3.69; Day 1B: 81.7 ± 3.80; Day 5A: 89.7 ± 3.04; Day 5B: 86.4 ± 3.18; Day

9A: 80.6 ± 9.64; Day 9B: 75.6 ± 7.09; Th-Cre$^{LC\text{-}DG}$::ArchT: Day 1A: 81.4 ± 3.01; Day 1B: 79.1 ± 5.67; Day 5A: 86.6 ± 5.06; Day 5B: 75.5 ± 4.42; Day 9A: 88.8 ± 3.30; Day 9B: 70.7 ± 6.16; Two-way ANOVA for Th-Cre$^{LC\text{-}DG}$::ArchT vs ArchT(−), A vs B: Day 1: Group: $F_{(1, 13)} = 0.025$, p = 0.878; Context: $F_{(1,13)} = 0.014$, p = 0.907; Group × Context: $F_{(1,13)} = 0.256$, p = 0.621; Day 5: Group: $F_{(1, 13)} = 2.464$, p = 0.141; Context: $F_{(1,13)} = 4.804$, p = 0.047; Group × Context: $F_{(1,13)} = 1.435$, p = 0.252; Day 9: Group: $F_{(1,13)} = 0.027$, p = 0.871; Context: $F_{(1,13)} = 17.03$, p = 0.001; Group × Context: $F_{(1,13)} = 5.39$, p = 0.037). Both groups received optogenetic light during trial, shaded bar denotes successful stimulation of opsin. All data are mean ± SEM. ***$p < 0.005$.

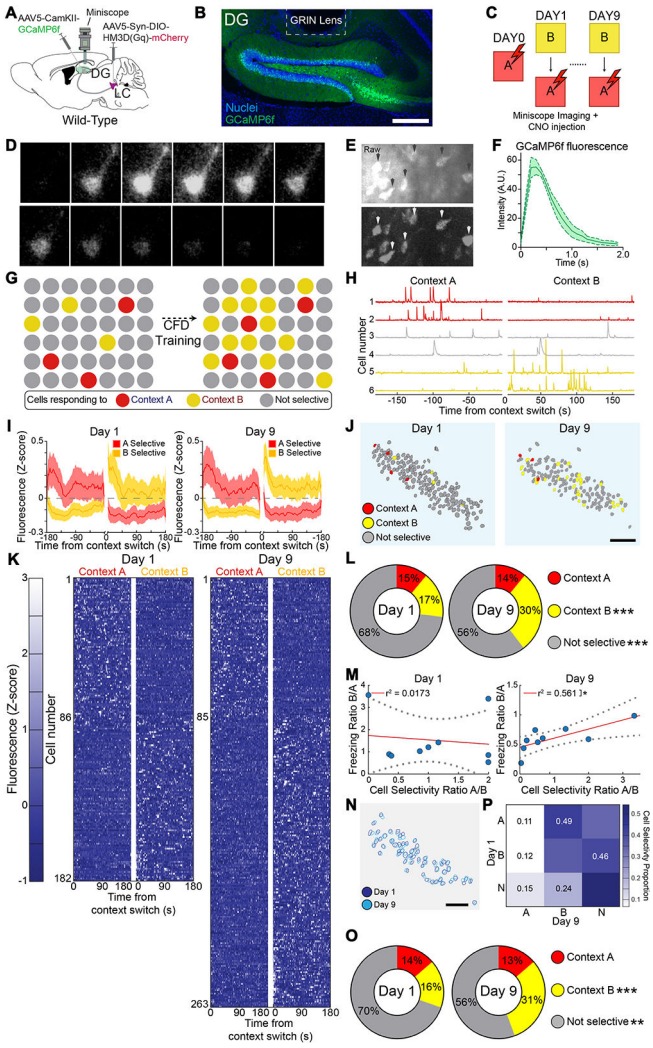

Fig. 2. Imaging of DG neural ensemble activity during contextual fear discrimination.

(**A**) Schematic of experimental approach depicts Ca^{2+} indicator (GCaMP6f) injected into the DG, and a microendoscopic GRIN lens implanted above the DG (**B**) Representative image depicting expression of GCaMP6f in the DG driven by CaMKII promoter and location of GRIN lens implant. Scale bar = 100 μm. (**C**) CFD with CNO injection 30 minutes prior to task and imaging during task. (**D**) Time-lapse image sequence of GCaMP6f fluorescence in an individual neuron. (**E**) Example of raw and dF/F *in vivo* epifluorescence images. (**F**) Intensity measurement of fluorescence dynamics from $GCaMP6f^{+}$ neurons ($n = 6$). (**G**) Schematic depicts hypothetical ensemble changes in the DG during CFD training. (**H**) Representative neurons responding selectively to context A (unsafe, top), context B (safe, bottom), or responding nonselectively (middle). (**I**) Averaged cell activity traces during days 1 and 9 of CFD task for neurons responding selectively to context A or context B. (**J**) Representative map of changes in context selectivity from day 1 (left) to 9 (right) of training in wild-type mice. (**K**) Fluorescence maps of cells identified from wild-type mice as responding selectively to context A (unsafe) and context B (safe) during days 1 (left) and 9 (right) of training (n = 9). There was a minimum 3-hour gap between exposure to context

B and context A. Cells were classified using a two-tailed *t*-test comparing Z-normalized fluorescence during the first 180 seconds in each context during Days 1 and 9. (**L**) Distribution of cells responding selectively to A, selectively to B, or nonselectively between days 1 and 9 of training (Chi-squared for selectivity: Context A: Chi-square = 0.168, Bonferonni adj. p-value ($p < 0.008$) = 0.682; Context B: Chi-square = 27.3, Bonferonni adj. p-value ($p < 0.008$) < 0.001; Nonselective: Chi-square = 18.1575, Bonferonni adj. p-value ($p < 0.008$) < 0.001). (**M**) Linear regression using Pearson correlation for ratio of cell selectivity between context A and context B vs. ratio of freezing behavior between context A and context B (Pearson correlation for cell selectivity ratio vs. freezing ratio: Day 1: $r = -0.132$, $r^2 = 0.0173$, $p = 0.737$; Day 9: $r = 0.749$, $r^2 = 0.561$, $p = 0.0202$). (**N**) Schematic depicting matching of reliably tracked neurons recorded both at the beginning and end of training. (**O**) Representation of shifts in cell selectivity between Day 1 and Day 9 of CFD training in reliably tracked neurons. (**P**) Distribution of cells identified at both the beginning and end of training responding selectively to A, selectively to B, or nonselectively between days 1 and 9 of training (Chi-squared for selectivity: Context A: Chi-square = 0, Bonferonni adj. p-value ($p < 0.008$) = 1; Context B: Chi-square = 13.9, Bonferonni adj. p-value ($p < 0.008$) < 0.001; Nonselective: Chi-square = 7.54, Bonferonni adj. p-value ($p < 0.008$) = 0.006. All data are mean ± SEM. $*p < 0.05$, $**p < 0.01$, $***p < 0.005$.

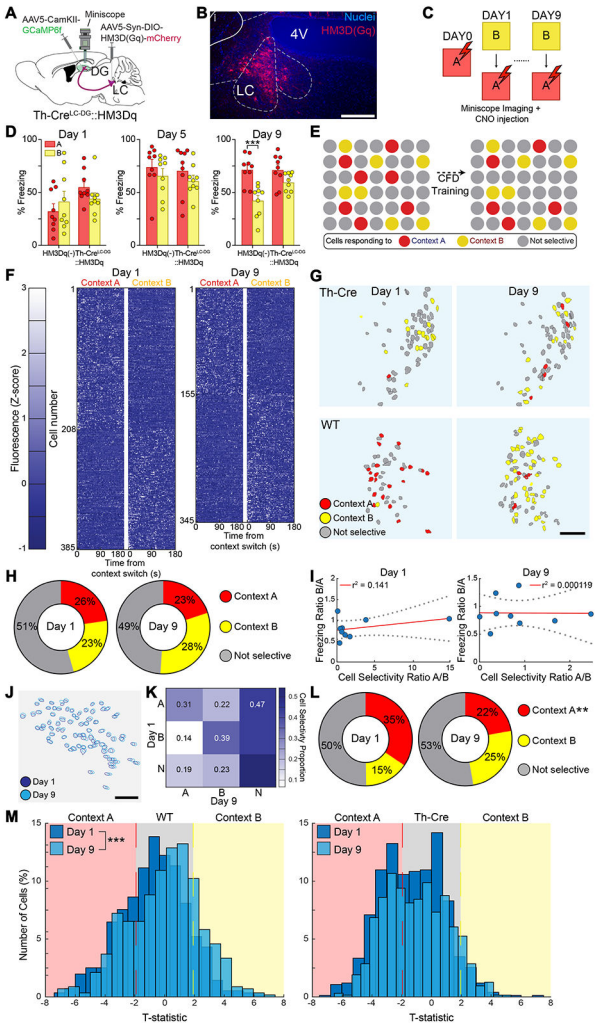

Fig. 3. Chemogenetic activation of LC-NE neurons alters DG neural ensemble activity during contextual fear discrimination.

(**A**) Schematic of experimental approach depicts infection of LC-NE cells using Th-Cre mouse line with DREADD system activating HM3Dq signaling chemogenetically (Th-Cre$^{LC\text{-}DG}$::HM3Dq), as well as Ca^{2+} indicator (GCaMP6f) injected into the DG, and microendoscopic GRIN lens implanted above the DG. (**B**) Representative image depicting expression of HM3Dq in LC-NE cells of Th-Cre mice. Scale bar = 50 μm (**C**) CFD task with CNO injection 30 minutes prior to task and imaging during task. (**D**) Chemogenetic activation of the LC-NE system impairs behavioral pattern separation in mice expressing HM3Dq in LC-DG projections (Th-Cre$^{LC\text{-}DG}$::HM3Dq, n = 9), but not in wild-type controls (HM3Dq(−), n = 9). HM3Dq(−) controls were able to discriminate on the ninth day of training, while Th-Cre$^{LC\text{-}DG}$::HM3Dq mice were unable to discriminate during the training (HM3Dq(−): Day 1A: 32.2 ± 6.40; Day 1B: 41.7 ± 9.34; Day 5A: 74.4 ± 6.99; Day 5B: 66.2 ± 6.37; Day 9A: 71.8 ± 4.52; Day 9B: 42.3 ± 5.03;Th-Cre$^{LC\text{-}DG}$::HM3Dq: Day 1A: 55.3 ± 4.97; Day 1B: 44.3 ± 5.61; Day 5A: 71.4 ± 7.55; Day 5B: 61.7 ± 4.81; Day 9A: 71.6 ± 4.97; Day 9B: 59.9 ± 2.94; Two-way ANOVA for Th-Cre$^{LC\text{-}DG}$::HM3Dq vs HM3Dq(−), A vs B: Day 1: Group: $F_{(1,16)}$ = 2.15, p = 0.162; Context: $F_{(1,16)}$ = 0.0566, p = 0.815; Group

× Context: $F_{(1,16)}$ = 5.20, p = 0.0366; Day 5: Group: $F_{(1,16)}$ = 0.207, p = 0.655; Context: $F_{(1,16)}$ = 5.06, p = 0.0389; Group × Context: $F_{(1,16)}$ = 0.0392, p = 0.846; Day 9: Group: $F_{(1,16)}$ = 3.46, p = 0.0811; Context: $F_{(1,16)}$ = 23.82, p = 0.0002; Group × Context: $F_{(1,16)}$ = 4.497, p = 0.0499). (**E**) Schematic depicts hypothetical ensemble changes in the DG during CFD training following activation of LC-NE system. (**F**) Fluorescence maps of neurons identified from Th-Cre mice as responding selectively to context A (unsafe) and context B (safe) during days 1 (left) and 9 (right) of training (n = 9). There was a minimum 3-hour gap between exposure to context B and context A. Cells were classified using a two-tailed *t*-test comparing Z-normalized fluorescence during the first 180 seconds in each context during Days 1 and 9. (**G**) Representative map of changes in context selectivity from day 1 (left) to 9 (right) of training in Th-Cre mice following activation of LC-NE system (top) and in wild-type mice (bottom). (**H**) Distribution of cells responding selectively to context A, selectively to context B, or nonselectively during days 1 and 9 of training (Chi-squared for selectivity: Context A: Chi-square = 2.35, Bonferonni adj. p-value (p < 0.008) = 0.125; Context B: Chi-square = 6.16, Bonferonni adj. p-value (p < 0.008) = 0.0131; Nonselective: Chi-square = 0.683, Bonferonni adj. p-value (p < 0.008) = 0.006). (**I**) Linear regression using Pearson correlation for ratio of cell selectivity between context A and context B vs. ratio of freezing behavior between context A and context B (Pearson correlation for cell selectivity ratio vs. freezing ratio: Day 1: r = 0.375, r^2 = 0.141, p = 0.32; Day 9: r = −0.109, r^2 = 0.0001, p = 0.98). (**K**) Representation of shifts in cell selectivity between Day 1 and Day 9 of CFD training in reliably tracked neurons. (**L**) Distribution of cells identified at both the beginning and end of training responding selectively to A, selectively to B, or nonselectively between days 1 and 9 of training (Chi-squared for selectivity: Context A: Chi-square = 8.82, Bonferonni adj. p-value (p < 0.008) = 0.003; Context B: Chi-square = 6.98, Bonferonni adj. p-value (p < 0.008) = 0.0082; Nonselective: Chi-square = 0.307, Bonferonni adj. p-value (p < 0.008) = 0.580). (**M**) Normalized distribution of all identified neurons in wild-type controls (left) and Th-$Cre^{LC\text{-}DG}$::HM3Dq mice (right) during days 1 and 9 of training (Kolmogorov-Smirnov test between Days 1 and 9: HM3Dq(−): K-stat = 0.171, p < 0.001; Th-$Cre^{LC\text{-}DG}$::HM3Dq: K-stat = 0.0724, p = 0.0533). All data are mean ± SEM. **p* < 0.05, ***p* < 0.01, ****p* < 0.005.

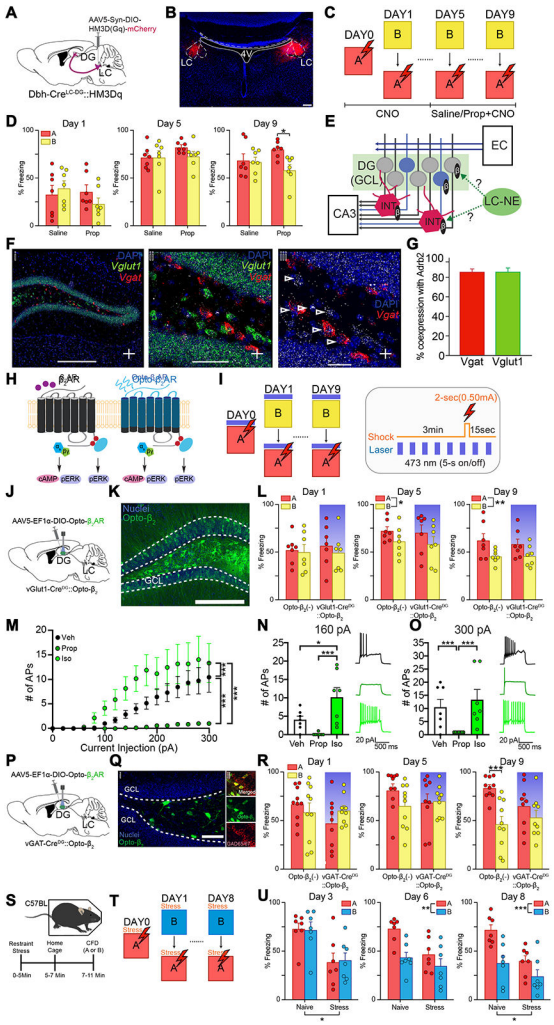

Fig. 4. Pharmacological and optogenetic modulation of noradrenergic signaling in DG interneurons and GCs during contextual fear discrimination.

(**A**) Schematic of experimental approach depicts infection of LC-NE cells using Dbh-Cre mouse line with DREADD system activating HM3Dq signaling chemogenetically. (**B**) Representative image depicting expression of HM3Dq in LC-NE cells of Dbh-Cre mice. Scale bar = 50 μm. (**C**) CFD task with CNO injection 30 minutes prior to task. Starting on day 5, animals received injection of either saline (Dbh-Cre::Saline) or propranolol (Dbh-Cre::Prop) 30 minutes prior to CNO injection. (**D**) Chemogenetic activation of the LC-NE system impairs behavioral pattern separation in mice receiving saline prior to CNO (n = 7), but not in those that received propranolol prior to CNO (n = 7). Animals receiving propranolol prior to CNO were able to successfully discriminate on the ninth day of training, but animals receiving saline prior to CNO were not (Saline: Day 1A: 33.3 ± 8.94; Day 1B: 39.8 ± 6.93; Day 5A: 71.4 ± 4.46; Day 5B: 71.8 ± 6.74; Day 9A: 68.3 ± 6.98; 9B: 66.9 ± 4.79; Propranolol: Day 1A: 35.8 ± 6.90; Day 1B: 22.8 ± 6.31; Day 5A: 82.5 ± 2.24; Day 5B: 73.3 ± 4.83; Day 9A: 80.0 ± 3.19; Day 9B: 59.1 ± 5.50; Two-way ANOVA for Saline vs Propranolol, A vs B: Day 1: Group: $F_{(1,12)} = 0.665$, $p = 0.431$; Context: $F_{(1,12)} = 0.361$, $p = 0.559$; Group × Context: $F_{(1,12)} = 3.29$, $p = 0.0947$; Day 5: Group: $F_{(1,12)} =$

1.31, p = 0.274; Context: $F_{(1,12)}$ = 1.15, p = 0.305; Group × Context: $F_{(1,12)}$ = 1.39, p = 0.261; Day 9: Group: $F_{(1,12)}$ = 0.109, p = 0.747; Context: $F_{(1,12)}$ = 6.34, p = 0.0271; Group × Context: $F_{(1,12)}$ = 4.78, p = 0.0494). (**E**) Diagram depicts hypothesis regarding potential LC-DG circuitry. Neurons in the Entorhinal Cortex (EC) send projections to the DG through the perforant pathway. The DG sends projections to pyramidal cells in the CA3 through mossy fibers. LC-NE projections may modulate granule cells (GC) directly during a new experience, or may modulate local interneurons (INT), causing strong tonic inhibition of GCs. (**F**) *In-situ* hybridization depicting coronal images of colocalization of *Adrb2* (white), *Vglut1* (green), and *Vgat* (red) within the DG of wild-type mice. (**G**) Quantification of *Vgat* and *Vglut1* coexpression with Adrb2. (**H**) Diagram depicts intracellular pathway of Opto-β_2 adrenergic receptors (ARs). (**I**) CFD task with optogenetic β_2-AR modulation of DG GCs or interneurons (left). Pattern of laser stimulation and shock (only in context A) during CFD (right). (**J**) Schematic of experimental approach depicts infection of DG GCs using vGlut1-Cre mouse line with chimeric light-sensitive adrenergic receptors (vGlut1-Cre^{DG}::Opto-β_2). (**K**) Opto-β_2 ARs were expressed in the GCL. Scale Bar = 200 μm (**L**) Acute photoactivation of Opto-β_2 ARs in DG GCs did not impair discrimination in mice expressing Opto-β_2 in LC-DG projections or wild-type controls. Opto-β_2(−) controls (n = 7) were able to discriminate on the ninth day of training, and vGlut1-Cre^{DG}::Opto-β_2 mice (n = 7) were also able to discriminate on the ninth day of training (Opto-β2(−): Day 1A: 52.2 ± 5.64; Day 1B: 49.7 ± 7.97; Day 5A: 72.2 ± 4.20; Day 5B: 61.3 ± 5.82; Day 9A: 62.0 ± 7.09; Day 9B: 45.6 ± 2.68; vGlut1-Cre^{DG}::Opto-β2: Day 1A: 56.9 ± 8.37; Day 1B: 49.2 ± 7.55; Day 5A: 70.4 ± 7.88; Day 5B: 58.3 ± 7.87; Day 9A: 58.1 ± 5.58; Day 9B: 45.6 ± 4.07; Two-way ANOVA for vGlut1-Cre^{DG}::Opto-β2 vs Opto-β2 (−), A vs B: Day 1: Group: $F_{(1, 12)}$ = 0.0468, p = 0.832; Context: $F_{(1,12)}$ = 1.49, p = 0.246; Group × Context: $F_{(1,12)}$ = 0.398, p = 0.540; Day 5: Group: $F_{(1, 12)}$ = 0.0913, p = 0.768; Context: $F_{(1,12)}$ = 5.20, p = 0.0417; Group × Context: $F_{(1,12)}$ = 0.0151, p = 0.904; Day 9: Group: $F_{(1, 12)}$ = 0.101, p = 0.757; Context: $F_{(1,12)}$ = 16.14, p = 0.0017; Group × Context: $F_{(1,12)}$ = 0.310, p = 0.588). Both groups received optogenetic light during trial, shaded bar denotes successful stimulation of opsin. (**M**) Whole-cell patch clamp recordings of depolarization elicited action potential firing. 5μM Isoproterenol increased (p<0.0001) while 50μM Propranolol decreased (p<0.0001) the number of depolarization elicited action potentials (Depolarization Step: $F_{(15,288)}$ = 9.303, p<0.0001; Drug: $F_{(2,288)}$ = 59.84, p<0.0001; Depolarization Step x Drug: $F_{(30,288)}$ = 2.207, p = 0.0005). (**N**) Comparison of action potential firing between vehicle, isoproterenol, and propranolol at 160 pA depolarization step (Derived from Fig. 4I: Veh vs Iso: p=0.0385; Prop vs Iso: p=0.0005). (**O**) Comparison of action potential firing between vehicle, isoproterenol, and propranolol at 300 pA depolarization step (Derived from Fig. 4I: Veh vs Prop: p=0.0007; Veh vs Iso: p=0.2752; Prop vs Iso: p<0.0001). (**P**) Schematic of experimental approach depicts infection of DG interneurons using vGAT-Cre mouse line with chimeric light-sensitive adrenergic receptors (vGAT-Cre^{DG}::Opto-β_2). (**Q**) Opto-β_2 ARs were expressed in the hilus area (left) and co-expressed with GAD67 (right). Scale Bars = 50 μm (left), 15 μm (right). (**R**) Acute photoactivation of Opto-β2 ARs in DG interneurons impaired discrimination in mice expressing Opto-β_2 in LC-DG projections but not in wild-type controls. Opto-β_2(−) controls (n = 10) were able to discriminate on the ninth day of training, while vGAT-Cre^{DG}::Opto-β_2 mice (n = 9) were not able to discriminate throughout the training (Opto-β2(−): Day 1A: 67.1 ± 5.63; Day 1B: 58.7 ±

9.36; Day 5A: 81.2 ± 6.50; Day 5B: 65.2 ± 7.25; Day 9A: 83.6 ± 3.41; Day 9B: 46.3 ± 7.96; vGAT-Cre^{DG}::Opto-β2: Day 1A: 47.3 ± 8.48; Day 1B: 60.5 ± 4.97; Day 5A: 68.5 ± 8.90; Day 5B: 70.1 ± 5.27; Day 9A: 65.1 ± 7.92; Day 9B: 53.4 ± 7.11; Two-way ANOVA for vGAT-Cre^{DG}::Opto-β_2 vs Opto-β_2(−), A vs B: Day 1: Group: $F_{(1, 17)} = 0.862$, p = 0.366; Context: $F_{(1,17)} = 0.352$, p = 0.561; Group × Context: $F_{(1,17)} = 7.167$, p = 0.016; Day 5: Group: $F_{(1, 17)} = 0.196$, p = 0.664; Context: $F_{(1,17)} = 2.175$, p = 0.159; Group × Context: $F_{(1,17)} = 3.281$, p = 0.088; Day 9: Group: $F_{(1,17)} = 0.407$, p = 0.531; Context: $F_{(1,17)} = 44.286$, p < 0.001; Group × Context: $F_{(1,17)} = 12.026$, p = 0.003). Both groups received optogenetic light during trial, shaded bar denotes successful stimulation of opsin. (**S**) Depiction of experimental protocol. Wild-type mice either received restraint stress or were handled normally for approximately 5 minutes, then placed back in the home cage for another 5 minutes prior to contextual fear discrimination (CFD) training. (**T**) CFD task with restraint stress administration replacing optogenetic activation. (**U**) Analysis of progressive days of training show that naïve animals successfully began to discriminate context A from context B, while stress-treated animals were unable to successfully discriminate. Additionally, stress-treated animals showed significantly lower freezing levels than naïve animals in the early part of training. However, significant differences are seen at the end of training (Day 3: Group: $F_{(1,9.76)} = 6.137$, p = 0.033; Day 6: Group: $F_{(1,9.46)} = 4.044$, p = 0.073; Context: $F_{(1,13.8)} = 21.429$, p < 0.001; Days × Context: $F_{(1, 13.8)} = 3.824$, p = 0.071; Day 8: Group: $F_{(1,10.39)} = 7.109$, p = 0.023; Context: $F_{(1,14.87)} = 24.6072$, p < 0.001; Days × Context: $F_{(1, 14.87)} = 3.322$, p = 0.085). All data are mean ± SEM. *p < 0.05, ***p < 0.005.

Key Resources Table

REAGENT or RESOURCE	SOURCE	IDENTIFIER
Antibodies		
anti-GAD65	Millipore	Cat#AB1511
Anti-GAD67	Millipore	Cat#MAB5406
Anti-TH	Millipore	Cat#AB152
Alexa Fluor 568-conjugated goat anti-rabbit	Invitrogen	Cat#A11011
Alexa Fluor 568-conjugated goat anti-chicken	Invitrogen	Cat#A11041
Alexa Fluor 633-conjugated goat anti-chicken	Invitrogen	Cat#A21103
Bacterial and Virus Strains		
AAV5-EF1α-DIO-ChR2-eYFP	WUSTL Hope Center Viral Core	N/A
AAV2 retro-EF1a-DIO-eYFP	WUSTL Hope Center Viral Core	N/A
AAV5-EF1α-DIO-eYFP	WUSTL Hope Center Viral Core	N/A
AAV5-EF1α-DIO-ArchT-eGFP	WUSTL Hope Center Viral Core	N/A
AAV5-EF1α-DIO-Opto-β_2AR-YFP	WUSTL Hope Center Viral Core	N/A
AAV5-FLEX-SaCas9-sgRNA-ADRB2-73-4	WUSTL Hope Center Viral Core	N/A
AAV5-CaMKIIα-GcAMP6f	Penn Vector Core	N/A
AAV5-Syn-DIO-HM3D(Gq)-mCherry	Addgene	N/A
Chemicals, Peptides, and Recombinant Proteins		
Clozapine-N-Oxide (CNO)	Sigma-Aldrich	Cat#C0832
Propranolol hydrochloride	Tocris Bioscience	Cat#0624
Isoproterenol hydrochloride	Tocris Bioscience	Cat#1747
VECTASHIELD Hardset Antifade Mounting Medium	Vector Laboratories	Cat#H-1400
Critical Commercial Assays		
RNAscope Fluorescent Multiplex Kit 2.0	Advanced Cell Diagnostics	Cat#320850
Wash Buffer Reagents	Advanced Cell Diagnostics	Cat#310091
Protease III & IV Reagents	Advanced Cell Diagnostics	Cat#322340
eGFP	Advanced Cell Diagnostics	*Cat#400281*
Experimental Models: Organisms/Strains		
Mouse: vGAT-IRES-Cre (*Slc32a1*$^{tm2(cre)Lowl}$/J)	The Jackson Laboratory	Stock #016962
Mouse: TH-IRES-Cre (Th$^{tm1(cre)Te}$/Kieg)	Infrafrontier	EM:00254
Mouse: vGlut1-IRES-Cre (Slc17a7$^{tm1.1(cre)Hze}$/J)	Bred in house	Gift from Larry Zweifel
Mouse: Dbh-Cre (Dbh$^{tm3.2(cre)Pjen}$/J)	Bred in house	Gift from Patricia Jensen (NIEHS)
Software and Algorithms		
Image processing, cell counter module	ImageJ/Fiji	https://imagej.net/Fiji
Graphpad Prism 8.0	GraphPad Software	https://www.graphpad.com/scientificsoftware/prism/
Illustrator CS6	Adobe	https://www.adobe.com/products/illustrator.html
EthoVision XT 10	Noldus	https://www.noldus.com/animal-behavior-research/products/ethovision-xt

REAGENT or RESOURCE	SOURCE	IDENTIFIER
MATLAB	MathWorks	https://www.mathworks.com/
Leica LAS X	Leica Microsystems	https://www.leica-microsystems.com/products/microscope-software/p/leica-las-x-ls/
Med-PC V Software Suite	Med-Associates, Inc.	https://www.med-associates.com/med-pc-v/
Video Freeze	Med-Associates, Inc.	https://www.med-associates.com/product/video-fear-conditioning/
nVista	Inscopix	https://www.inscopix.com/nVista